

TESTING AN ENTROPY ESTIMATOR RELATED TO THE DYNAMICAL STATE OF GALAXY CLUSTERS

J. M. Zúñiga,¹ C. A. Caretta,¹ A. P. González,² and E. García-Manzanárez¹

Received ; accepted

RESUMEN

Proponemos el estimador de entropía H_Z , calculado a partir de parámetros dinámicos globales, en un intento de capturar el grado de evolución de los sistemas de galaxias. Asumimos que las distribuciones (espaciales y de velocidad) observadas de galaxias miembros en estos sistemas evolucionan en el tiempo hacia estados de mayor relajación dinámica (mayor entropía), volviéndose más aleatorias y homogéneas en el equilibrio virial. Así, la entropía H_Z debería corresponder con el estado de ensamblaje gravitacional de los sistemas. Esto se probó en una muestra de 70 cúmulos bien muestreados del Universo Local cuyo estado de ensamblaje gravitacional, clasificado a partir del análisis óptico y de rayos X de las subestructuras, muestra una clara correlación estadística con H_Z . Este estimador también fue testeado sobre una muestra de cúmulos (halos) de las simulaciones IllustrisTNG, obteniendo resultados acordes con los obtenidos para los cúmulos observados.

ABSTRACT

We propose the entropy estimator H_Z , calculated from global dynamical parameters, in an attempt to capture the degree of evolution of galaxy systems. We assume that the observed (spatial and velocity) distributions of member galaxies in these systems evolve over time towards states of higher dynamical relaxation (higher entropy), becoming more random and homogeneous in virial equilibrium. Thus, the H_Z -entropy should correspond to the gravitational assembly state of the systems. This was probed in a sample of 70 well sampled clusters in the Local Universe whose gravitational assembly state, classified from optical and X-ray analysis of substructures, shows clear statistical correlation with H_Z . This estimator was also tested on a sample of clusters (halos) from the IllustrisTNG simulations, obtaining results in agreement with the observational ones.

Key Words: galaxies: clusters: general — galaxies: statistics — galaxies: kinematics and dynamics — gravitation — equation of state

1. INTRODUCTION

Galaxies are not uniformly distributed in the Universe, instead they undergo gravitational clustering that leads to an intricate three-dimensional structure in the shape of a network of knots, filaments, walls and voids (*e.g.*, Libeskind et al. 2018). This cosmic web, revealed in both the observed distribution of galaxies (*e.g.*, Geller & Huchra 1989; Santiago-Bautista et al. 2020) and in cosmological simulations (*e.g.*, Davis et al. 1985; Springel et al. 2005), is called the Large-Scale Structure of the Uni-

verse (LSS, *e.g.*, Peebles 1980; Einasto 2010), and contains systems of galaxies at different scales embedded in it (*e.g.*, Einasto et al. 1984; Cautun et al. 2014). Such systems go from small groups, like the Local Group that hosts the Milky Way, to superclusters, the largest and youngest coherent structures formed under gravitational influence in the Universe (reaching up to ~ 100 Mpc long, *e.g.*, Oort 1983; Böhringer & Chon 2021).

Knot-shaped regions, that is, quasi-spherical overdensities of galaxies with radii ranging from ~ 1.0 to ~ 5.0 Mpc, are commonly known as galaxy groups or clusters. If we define these galaxy systems richness in terms of galaxies with masses of the order

¹Departamento de Astronomía, Universidad de Guanajuato, México.

²Departamento de Matemáticas, Universidad del Cauca, Colombia

of the Milky Way or greater, it is usually considered that groups have between 3 and 30 galaxies, poor clusters have between 30 and 50 galaxies, and rich clusters have more than 50 galaxies, counting them over a projected sky area of radius $R_A \sim 2.1$ Mpc according to the criteria first proposed by Abell (1958) (see also, Abell et al. 1989; Bahcall 1996). However, this classification is only an *ad hoc* criterion since there is actually a continuum in the richness of these systems and their physical limits are uncertain. A more elegant and physically motivated way to characterize clusters is to define them based on their expected virialized zones, that is, as galaxy regions where the mean density is Δ_c times the critical density of the Universe at the considered redshift (typical values are $\Delta_c \sim 100 - 200$, *e.g.*, Carlberg et al. 1997b; Bryan & Norman 1998; Tully 2015), which provides better estimates of their mean dimensions and dynamical properties in the cosmology used.

The baryonic —stellar and gaseous— matter contained in galaxies and in the form of intracluster X-ray emitting hot gas (intracluster medium, ICM, *e.g.*, Böhringer & Werner 2010) is estimated (*e.g.*, White 1992; Lima-Neto et al. 2005) to account for only 15% of the total mass of a galaxy system, while the remaining 85% are provided by the dark matter (DM). Nevertheless, in a first approximation, one can consider a group/cluster as a collisionless ensemble of galaxies moving in the mean gravitational field generated by its total mass (*e.g.*, Schneider 2015). In this context, galaxies may be taken as fundamental observational tracers (or primary units, *e.g.*, Padmanabhan 1993) of the global dynamical properties of the galaxy system.

The process of formation and evolution of a cluster from a matter density perturbation to a galaxy system in dynamical equilibrium is driven both by the initial cosmological conditions and by various physical and stochastic mechanisms (*e.g.*, Binney & Tremaine 2008). Initially, both the homogeneous background and the matter perturbation expand with the Hubble flow; however, a fraction of this matter condenses into a set of galaxies that decouple from the expansion. The cluster, itself, in the course of time, decouples from the expansion, forming now a gravitationally bound system, which turns around and begins a process of collapse that ends in an eventual virialization (*e.g.*, Gunn & Gott III 1972). This is a state of statistical equilibrium of internal gravitational forces, reflected in the averages of the total kinetic and potential energies of galaxies (*e.g.*, Limber & Mathews 1960). Analyzing the transitory evolutionary state of galaxy systems is

not a trivial task, even when gravity is the sole driving force shaping their evolutionary processes. Here, we use the term ‘evolutionary state’ to refer to the degree of progress a galaxy system has in its evolutionary line, starting from its formation and ending at equilibrium (relaxation).

In this work we present a method to characterize the evolutionary state of galaxy systems by estimating the entropy component that depends only on the macroscopic state of their galaxy ensembles. For this, we propose a specific entropy estimator (H_Z) that combines (optical) observational parameters of the systems such as virial mass, volume, and galaxy velocity dispersion. Our fundamental premise is that a galaxy ensemble should evolve in the sense of increasing entropy, modifying its distribution of galaxies in the observed phase-space (which includes radial, angular and velocity coordinates) to a more random and dynamically relaxed one where there are no macroscopic movements or special configurations (*e.g.*, Landau & Lifshitz 1980; Saslaw & Hamilton 1984). This means that the spatial and velocity distributions of member galaxies change as the system evolves, starting from more substructured ensembles (with less entropy) towards more homogeneous ones in dynamical relaxation (with higher entropy). Of course, the parameters associated with the global dynamics of the system also change in the process, and may be useful for the estimation of state functions such as entropy. No assumption is made here about the distribution of DM and ICM within the cluster (*e.g.*, Lokas & Mamon 2003; Lima-Neto et al. 2005), but only their important contribution to the total gravitational potential that determines the dynamics of the galaxy ensemble.

To evaluate the H_Z -entropy estimator we make use of different tests. The first is the comparison between H_Z -entropy estimator and a discrete classification of assembling states applied to an observational samples of 70 nearby clusters ($z \lesssim 0.15$). The second test is the calculation of the Shannon entropy, which provides a quantitative measure of the degree of disorder (or uncertainty) in the distribution of galaxies at different regions within each cluster phase-space. Substructures are considered as special configurations and their presence reduces the Shannon entropy, so more relaxed systems (with a more random galaxy distribution in the phase-space) are expected to have higher entropies. In this test, galaxy systems are considered as data sets whose information entropies can be calculated. Both the observational cluster sample and another from simulated cluster halos, with their respective subhalos, are used to

compare H_Z and Shannon entropies. As complementary validations, different approaches are used, including the analysis of the relaxation probability of the systems (based on statistical distances between empirical and reference galaxy distributions) and the study of correlations between H_Z and other continuous parameters commonly associated to the dynamical state of the systems.

In Section 2, we extend the discussion about the dynamical equilibrium and stability of galaxy clusters, together with a brief description of the way evolutionary state is commonly characterized from observed and simulated data. In Section 3, we focus on the entropy-based estimator and present our proposal to quantify the dynamical state of galaxy systems. In Section 4, we apply our method to a sample of 70 well-sampled galaxy clusters, from very rich to poor ones, in the nearby Universe. In Section 5 we calculate the Shannon entropy for both the observational sample and a sample of 248 cluster halos from the IllustrisTNG simulation. Then, we compare this parameter with H_Z . Other dynamical parameters are evaluated in Section 6 also for validating H_Z . Discussion and conclusions are presented in Section 7. Throughout this paper we assume a flat Λ CDM cosmology with the following parameters: Hubble constant $H_0 = 70 \text{ km s}^{-1} \text{ Mpc}^{-1}$, matter density $\Omega_M = 0.3$ and dark energy density $\Omega_\Lambda = 0.7$.

2. EVOLUTION, EQUILIBRIUM AND STABILITY OF GALAXY CLUSTERS

2.1. Reaching virial equilibrium

The evolution of galaxy systems at various scales is understood today through the hierarchical formation model (*e.g.*, Peebles 1980; Padmanabhan 1993; Zakhochay 2018) in a Λ CDM scenario. According to this model, the smallest systems (galaxy groups and poor clusters) merge —via gravity— to form the largest ones (rich clusters and superclusters), being the observed substructuring a consequence of this process. Subsequently, these galaxy ensembles undergo a non-linear gravitational collapse during which a combination of physical and stochastic mechanisms (*e.g.*, Lynden-Bell 1967; Saslaw 1980; Padmanabhan 1990) drive the systems into a further state of dynamical relaxation —the virial equilibrium— in which their substructures vanish (*e.g.*, Araya-Melo et al. 2009).

Galaxy clustering is an irreversible process where, as galaxies accumulate, different mechanisms tend to increase the number of ways in which, in a statistical sense, internal energy can be distributed within

the systems (*e.g.*, Saslaw 1980; Saslaw & Hamilton 1984). Once bound and during collapse, the galaxy system undergoes internal —dissipationless— processes (*e.g.*, violent relaxation, phase mixing, energy equipartition, galaxy mergers, fading of substructures and density or temperature gradients, among others, see, White 1996; Dehnen 2005; Binney & Tremaine 2008) that lead to states of greater dynamical relaxation. All these processes are dominated by gravitational interactions that, during the relaxation time, tend to homogenize the spatial distribution of the member galaxies and distribute their radial velocities in a Gaussian way —inside the clusters, galaxies are scattered randomly (achieving a quasi-Maxwellian velocity distributions as they tend to virialization, *e.g.*, Saslaw & Hamilton 1984; Sampaio & Ribeiro 2014), making the tendency for macroscopic motions to disappear. This requires the individualization of the motions of the galaxies, so that any substructure (*e.g.*, accreted groups) will be ‘dissolved’ before the cluster virializes. The thermodynamic perturbations and the changes in the distribution of the ICM inside the clusters during their evolution also produce increases in the total entropy of these systems (*e.g.*, Tozzi & Norman 2001; Voit 2005).

The equilibrium state can be understood, in first approximation, as that in which the gravitational collapse is supported by the effect of inertial —centrifugal or dispersion— forces, achieving relaxed internal configurations (called states of dynamical relaxation), that is, in which there are no unbalanced potentials, such as gravitational-driving forces, within galaxy systems. In this sense, collisionless systems in equilibrium are analogous to self-gravitating fluids because they support gravitational collapse through “pressure gradients” proportional to the velocity dispersion that, at each point, tend to disperse any local increase in particle density (*e.g.*, Binney & Tremaine 2008). Furthermore, dynamical equilibrium is characterized by the statistical equality of the cluster mass profiles obtained from different galaxy populations within the cluster (*e.g.*, Carlberg et al. 1997a), implying that all these populations are in equilibrium with the cluster potential according to the hydrodynamical equilibrium model by Jeans.

Throughout the evolution of an isolated cluster, its total internal energy $U = K + W$ is conserved so that, as the member galaxies get closer together (spontaneous reduction of inter-particle distance r_{ij} by mutual attraction), the gravitational potential energy W decreases (becoming more negative) and

consequently the total internal kinetic energy K increases. This is reflected observationally as an increase in the velocity dispersion of galaxies, which can stop the collapse. Thus, when the system finds some route to dynamical equilibrium, the increase in K at the expense of the decrease in W does not continue indefinitely, but evolves toward configurations in which the ratio

$$b = -\frac{W}{2K}, \quad (1)$$

tends to one ($b \rightarrow 1$, *e.g.*, Saslaw & Hamilton 1984; Binney & Tremaine 2008). The asymptotic limit, $b = 1$, of this tendency is the virial equilibrium:

$$W = -2K, \quad (2)$$

a state in which dynamical parameters that characterize the global configuration of the system remain, at least temporarily, stationary (relaxed). The virial theorem expresses a statistical equilibrium between the temporal averages of the total internal kinetic and gravitational potential energies, *i.e.*, $\langle W \rangle_\tau = -2\langle K \rangle_\tau$, but these energies are also the result of an ensemble of interacting galaxies (*e.g.*, Limber & Mathews 1960), so it is reasonable to approximate the temporal averages by the average of the ensemble expressed in (2). Virial equilibrium is assumed to be the type of dynamical equilibrium reached by self-gravitating systems.

2.2. Stability

Going beyond the description of equilibrium in galaxy systems, we need to discuss if this equilibrium is stable and this topic requires involving the concept of ‘entropy’. As any thermodynamic system, self-gravitating systems progress in the sense of increasing entropy (*e.g.*, Lifshitz & Pitaevskii 1981; Tremaine, Hénon & Lynden-Bell 1986; Pontzen & Governato 2013) towards the state of dynamical equilibrium described above. Galaxy clustering simulations also confirm this fact (*e.g.*, Saslaw & Hamilton 1984; Iqbal et al. 2006, 2011). Due to the scattering experienced by galaxies in the phase-space of clusters, these become the regions within the LSS where first-order entropy production occurs by increasing the randomness of the motion of galaxies during their gravitational accumulation. Even if galaxy clusters are isolated, some entropy is generated—or produced—due to the presence of internal irreversibilities. The peculiarity here is that the virial equilibrium is not unique, but only a *metastable equilibrium state* (*e.g.*, Antonov 1962; Lynden-Bell & Wood 1968; Padmanabhan 1990;

Chavanis et al. 2002). This means that the entropy of self-gravitating systems can grow indefinitely without reaching a global maximum, that is, the virial equilibrium is only a state of local extreme of entropy (*e.g.*, Padmanabhan 1989).

The dynamical equilibrium of a galaxy cluster can be disturbed if it actively interacts with its surroundings, for example through mergers with other clusters and/or group accretions or tidal forces. As a result, the cluster takes a route towards a new equilibrium, in a state of higher entropy. Concerning the impact of the interaction, if the accreted groups are very small, the clusters can be kept unperturbed in states close to equilibrium. In more extreme cases, the merger of two massive clusters completely removes the systems from their equilibrium. In dense environments, such as supercluster cores, the accretion of galaxies and groups by the most massive clusters continually disturbs their dynamical states. On the other hand, in less dense environments, such as along filaments or edges near voids, clumpy clusters evolve as quasi-isolated systems, reaching dynamical relaxation possibly faster, without many significant disturbances, but accessing lower entropy levels compared to clusters in “busy” environments. That is, depending on the cosmological environment inside the LSS in which a cluster evolves, its relaxation process may be affected several times—or not—given the amount of matter available in its surroundings.

The most stable states of a galaxy cluster—of mass \mathcal{M} and radius R —are favored when the density contrast between its center and its edge is $\rho_0/\rho(R) < 709$ and the internal energy is $U > -0.335G\mathcal{M}^2/R$ (the Antonov instability or gravothermal catastrophe, *e.g.*, Antonov 1962; Lynden-Bell & Wood 1968), and under these conditions the virial equilibrium corresponds to a local maximum of entropy (*e.g.*, Padmanabhan 1989, 1990). In fact, the most stable dynamical configurations that self-gravitating systems can access are those in which the particle—or matter—distribution settles on a core-halo structure (*e.g.*, Binney & Tremaine 2008; Chavanis et al. 2002). This theoretical structure, characterized by a collapsed core coexisting with a regular halo, has also been confirmed by simulations (*e.g.*, Cohn 1980; Balberg, Shapiro & Inagaki 2002) and recognized by the distributions of galaxies (*e.g.*, Sarazin 1988; Adami et al. 1998) and the ICM in observed clusters (*e.g.*, Tozzi & Norman 2001; Cavagnolo et al. 2009).

2.3. *Estimating the evolutionary state of galaxy systems*

Observationally, a cluster close to dynamical equilibrium is distinguished from a non-relaxed one by exhibiting a more regular morphology (*e.g.*, Sarazin 1988), both in the optical and X-rays, and a more homogeneous—projected—spatial distribution of member galaxies (without the presence of significant substructures, *e.g.*, Caretta et al. 2023, and references therein), as well as by having a more isotropic galaxy velocity distribution (or Gaussian in the line-of-sight, *e.g.*, Girardi & Mezzetti 2001; Sampaio & Ribeiro 2014).

Concerning global morphology, the most dynamically relaxed clusters tend to present low ellipticity shapes in the projected distribution of galaxies and X-ray surface brightness maps, with a—possible—single peak at their centers. Several morphological classifications have been proposed following this premise (*e.g.*, Sarazin 1988, and references therein). There are also indicators of the internal structure of the galaxy systems, such as the radial profile and the degree of concentration of galaxies (*e.g.*, Adami et al. 1998; Tully 2015; Kashibadze et al. 2020), as well as a measure of the presence of substructures within them using 1D, 2D and 3D tests (*e.g.*, Geller & Beers 1982; Dressler & Shectman 1988; Caretta et al. 2023).

In this sense, a significantly substructured system, either from optical observation of galaxy subclumps (*e.g.*, Geller & Beers 1982; Bravo-Alfaro et al. 2009; Caretta et al. 2023) or the detection of multiple peaks in X-ray emission (*e.g.*, Jones & Forman 1984; Buote & Tsai 1995; Laganá et al 2019), cannot be considered in dynamical equilibrium. Thus, the presence and significance of substructures reveal the far the galaxy system is from a relaxed and homogeneous global potential. A description of the cluster level of internal substructuring is called its gravitational assembly state (*e.g.*, Caretta et al. 2023).

In principle, one can also measure global parameters related to the internal dynamics (*e.g.*, Carlberg et al. 1996; Girardi & Mezzetti 2001)—or dynamical state—of the galaxy system. These parameters are associated, for example, with the mass, radius and velocity dispersion of the system. Such approach supposes that both the observable aspect and structure and the dynamical parameters of the system change in a correlated manner during its evolution, dominated by mechanisms that take it from more irregular and substructured configurations to those with more homogeneous galaxy

distributions and more dynamically relaxed (*e.g.*, Araya-Melo et al. 2009).

Furthermore, from X-ray observations one can construct entropy (or temperature or density) profiles that account for the evolutionary history, structure and thermodynamic state of the ICM inside the clusters (*e.g.*, Tozzi & Norman 2001; Voit 2005; Cavagnolo et al. 2009), which also contributes to the study of the degree of relaxation—or disturbance—of their gravitational potentials (analysis of self-similarity of clusters). Nevertheless, we are not always fortunate enough to detect X-ray emission from clusters nor to have the amount of data necessary to carry out massive studies, so for this we are still limited to optical surveys.

3. ENTROPY OF GALAXY SYSTEMS FROM GLOBAL PARAMETERS

Based on the ‘classical’ concept of entropy of a particle system, it is possible to construct an estimator for the entropy component related to the set of member galaxies of a cluster, the ‘galaxy ensemble’. The depth of the cluster’s global potential well, which determines how fast the bound galaxies must move, is proportional to the total mass of the cluster that can be estimated, with negligible bias (see, Biviano et al. 2006), by the virial mass estimator

$$\mathcal{M}_{\text{vir}} = \frac{\alpha\pi}{2G}\sigma_{\text{LOS}}^2 R_p, \tag{3}$$

where σ_{LOS} is the line-of-sight (LOS) velocity dispersion of the sampled galaxies, α is a deprojection parameter for σ_{LOS} assuming anisotropy in the galaxy velocity distribution ($\alpha = 3$ if orbits have an isotropic and isothermal distribution, *e.g.*, Tully 2015, and references therein), and

$$R_p = \frac{N(N-1)}{\sum_{k<l} 1/R_{kl}}, \tag{4}$$

is the projected mean radius of the distribution of cluster galaxies, where R_{kl} is the projected distance (in Mpc) between pairs of the N sampled galaxies. The factor $\pi/2$ in (3) is the radius deprojection factor (*e.g.*, Limber & Mathews 1960) so that statistically $R_{\text{vir}} \simeq \pi R_p/2$ is the three-dimensional virial radius of the cluster (*e.g.*, Carlberg et al. 1996; Girardi & Mezzetti 2001), a measure of the region of gravitational confinement of its member galaxies.

Now, in a first approximation, we can imagine the set of cluster galaxies as a system of particles with mean kinetic energy (*e.g.*, Schneider 2015)

$$K = \frac{\alpha}{2}\mathcal{M}_{\text{vir}}\sigma_{\text{LOS}}^2, \tag{5}$$

and confined in a region of volume

$$V = \frac{4}{3}\pi R_{\text{vir}}^3. \quad (6)$$

We assume that the velocity dispersion of galaxies is proportional to the ‘temperature’ T of the galaxy ensemble³, so that $\sigma_{LOS}^2 = \beta T$, with β being a proportionality constant that transforms temperature units into square velocity units. Furthermore, the mean ‘pressure’ of the galaxy ensemble, commonly approximated as $P = \bar{\rho}\sigma_{LOS}^2$, where $\bar{\rho}$ is the mean mass density of the system (*e.g.*, Schneider 2015), can be conveniently modified to the form $P = \bar{\rho}\sigma_{LOS}^2(1 - 2b)$, where the factor $(1 - 2b)$ has been introduced to generalize the expression (see, for example, Saslaw & Hamilton 1984). Thus, $P > 0$ for unbound systems ($b = 0$), just like an ordinary gas of particles enclosed in a hypothetical sphere of volume V with no gravitational potential; while $P < 0$ in self-gravitating bound systems ($b > 0.5$). The mean value of pressure in a marginal virial equilibrium ($b \rightarrow 1$), for a system with $\bar{\rho} = \mathcal{M}_{\text{vir}}/V$, is

$$P = -\bar{\rho}\sigma_{LOS}^2 = -\frac{2K}{\alpha V}, \quad (7)$$

matching the definition of the so-called gravitational pressure (*e.g.*, Padmanabhan 2000), $P = W/3V$, when $\alpha \rightarrow 3$.

In virial equilibrium, the internal energy of the galaxy ensemble is $U = K + W = -K$, according to (2). However, for any state of the system including those prior to equilibrium, the internal energy can be generalized, as in Saslaw & Hamilton (1984), in the form $U = K(1 - 2b)$, where, for unbound systems ($b = 0$) the internal energy is only kinetic, while for bound and virialized systems ($b \rightarrow 1$) we get the marginal value

$$U = -\frac{\alpha}{2}\mathcal{M}_{\text{vir}}\beta T, \quad (8)$$

where $\sigma_{LOS}^2 = \beta T$, as before. Note that the mean potential energy of the galaxy system does not appear explicitly in its ‘thermodynamic description’.

As can be inferred from (3), galaxy systems of fixed mass internally heat up (T increases) when they contract (R_{vir} decreases) and cool down (T decreases) when they expand (R_{vir} increases). In addition, from (8) it is possible to appreciate an atypical behavior of virialized self-gravitating systems. If we allow the galaxy systems to exchange energy—but not matter—with the environment, then they cool

³Thought, simplistically, as a system of point masses (particles).

down ($dT < 0$) by receiving energy ($dU > 0$) from the environment and warm up ($dT > 0$) by releasing energy ($dU < 0$) to it. These types of systems are said to have negative specific heats ($dU/dT < 0$, *e.g.*, Lynden-Bell D. & Lynden-Bell R. 1977).

A fundamental expression of the form $u = u(s, v)$, which relates the specific variables u , s and v of internal energy, entropy and volume respectively, must be satisfied by a single-component thermodynamic system (*e.g.*, Saslaw & Hamilton 1984). Differentiating, we get that $du = (\partial u/\partial s)_v ds + (\partial u/\partial v)_s dv$, obtaining the standard Gibbs Tds relation $du = Tds - Pdv$, with $T \equiv (\partial u/\partial s)_v$ and $P \equiv -(\partial u/\partial v)_s$ being respectively the temperature and pressure of the system. Let $u = U/\mathcal{M}_{\text{vir}}$, $\kappa = K/\mathcal{M}_{\text{vir}}$, $s = S/\mathcal{M}_{\text{vir}}$ and $v = V/\mathcal{M}_{\text{vir}}$ the specific variables per unit of mass for internal and kinetic energies, entropy and volume, respectively. It is evident that Gibbs Tds relation does not fit in its original form to self-gravitating systems. For ordinary systems of particles, both adiabatic compression ($dv < 0$) and isocoric heat input from the environment ($Tds > 0$) imply an increase in their internal energy ($du > 0$). Instead, for self-gravitating system of particles, compressions imply ‘heating’ ($dT, d\kappa > 0$), but with a decrease in internal energy ($du < 0$), which leads to an increase in the entropy of the system ($ds > 0$) according to the direction of the spontaneous process of gravitational accumulation.

It is necessary to use an expression analogous to the Gibbs Tds equation, but which conforms to the thermodynamic behaviour of self-gravitating systems described above. In the considered galaxy ensemble the entropy increases along with the internal kinetic energy as they virialize (see, section 2). Then, we can impose that, in systems of point galaxies, $s = s(\kappa, v)$ with differential form

$$ds = \left(\frac{\partial s}{\partial \kappa}\right)_v d\kappa + \left(\frac{\partial s}{\partial v}\right)_\kappa dv, \quad (9)$$

where, by analogy with the well-known thermodynamic expressions for temperature and pressure in the Gibbs Tds equation, we have

$$\left(\frac{\partial s}{\partial \kappa}\right)_v = \frac{1}{T}, \quad \text{and} \quad \left(\frac{\partial s}{\partial v}\right)_\kappa = \frac{P}{T}. \quad (10)$$

Note that, for self-gravitating galaxy systems in general, we need the $1/T > 0$ and $P/T < 0$ conditions to be satisfied. The last condition is required to obtain entropy increases during the gravitational collapse processes (in which the systems undergo contractions, $dv < 0$). This suggests a negative pressure

in this type of systems (like systems in phase transitions or metastable states in liquids, *e.g.*, Imre 2007) that causes a “repulsion” and prevents a singular collapse, just as proposed by the expression (7).

Finally, in order to obtain an estimator for the entropy of galaxy clusters, we will solve the system of differential equations (10) assuming that $1/T = \alpha\beta/2\kappa$ and $P/T = -\beta/v$, obtained by combining (5) and (7). Thus, the solution can be verified to be of the form

$$s(\kappa, v) = \beta \ln \left(\kappa^{\frac{\alpha}{2}} v^{-1} \right) + s_0, \quad (11)$$

where s_0 is an integration constant possibly related to the initial entropy of the galaxy ensemble, *e.g.*, the entropy it had when the distribution of galaxies was not yet concentrated before gravitational clustering (see, section 2). Replacing the expressions $\kappa = (\alpha/2)\sigma_{LOS}^2$ and $v = (4/3)\pi R_{vir}^3 \mathcal{M}_{vir}^{-1}$ in (11) we get the dimensionless estimator

$$H_Z \equiv \frac{s - s_0}{\beta} = \ln \left(\frac{\mathcal{M}_{vir}}{\frac{4}{3}\pi R_{vir}^3} \right) + \frac{\alpha}{2} \ln \left(\frac{\alpha}{2} \sigma_{LOS}^2 \right), \quad (12)$$

defined only in terms of observational parameters that can be obtained through optical data (*e.g.*, galaxy coordinates and redshifts).

4. TESTING THE H_Z ENTROPY ESTIMATOR IN GALAXY SYSTEMS

4.1. *Observational data*

We use data from Caretta et al. (2023), a sample of 67 galaxy clusters, from Abell/ACO (Abell 1958; Abell et al. 1989) catalogs, with redshifts up to $z \sim 0.15$. These clusters were selected because they are among the most well sampled galaxy systems in the nearby Universe, and cover roughly uniformly from poor to rich systems (with ICM-temperatures from 1 to 12 keV), being balanced for including all BM (Bautz & Morgan 1970) types. Three other non-Abell clusters with similar characteristics were included in our sample (AM0227-334, SC1329-313 and MKW03S), which allow us to call, for short, our observational sample *Top70* from now on (Table 1). For each cluster, a sample of spectroscopically confirmed member galaxies is available, selected inside the cluster caustics up to a fiducial aperture of $1.3 \times r_{200}$ from the centre of the cluster (chosen to be the Central Dominant Galaxy, CDG). The numbers of these presumably virialized members ranges from 21 to 919 (average 154), while originally at least 90 spectroscopic redshifts were available for each cluster (see Caretta et al. 2023, for the details of the

process for determining membership, caustics and virial radius). One should note that the richness of a cluster is related to both intrinsic and observational conditions —more massive clusters are richer, while nearby clusters tend to be preferentially observed. However, the numbers of members we have are adequate for minimizing observational biases in counting them in bins. Astrometric positions of galaxies have uncertainties of $\pm 0.25''$, and radial velocities of $\pm 60 \text{ km s}^{-1}$ (see, Caretta et al. 2023, and references therein).

By using different 1D, 2D and 3D methods (*e.g.*, Dressler & Shectman 1988), applied to the distribution of the members inside the caustics, these authors searched for optical substructures in the cluster sample, supplementing their analysis with X-rays and radio literature data. They found that at least 70% of the clusters in their sample present clear signs of substructuring, with 57% being significantly substructured. The significance of the identified substructures in each cluster was estimated by the fraction of galaxies they contain respect to the total richness.

The clusters were classified into five assembly state levels according to the presence —or not— and relative importance of substructures: unimodal systems, made up of a regular structure (U); low mass unimodal systems (L); systems with a primary structure and only low significance substructures (P); significantly substructured systems with one main substructure (S); and multimodal conglomerates with more than one main substructure (M). While the L clusters are young poor galaxy systems, representing evolutionary states prior to amalgamation processes but already relatively placidly evolved, the U clusters are old and massive, which have probably grown by mergers and accretions and have already settled close to a relaxation state. P clusters are also old and massive, but still present signs of recent accretions; since these accretions are minor, the relaxation state of the cluster is almost unaffected. Finally, S and M clusters are systems during merging processes, the difference being if these mergers are minor or major, respectively.

The benefit of using this sample lies in the availability of this discrete classification of gravitational assembly states (see Column 2 of Table 2 below). This will serve to establish correlations between H_Z estimator applied to the ensemble of galaxies of each cluster and the evolutionary state obtained from direct observational methods.

The observational cluster sample is reported in Table 1: Column 1 shows the name of clusters;

TABLE 1
CLUSTER SAMPLE (TOP70).

Name ^a	Optical data				X-ray data ^b		Basic properties		
	RA _{CDG} [deg] _{J2000}	Dec _{CDG} [deg] _{J2000}	\bar{z}	N_a	r_{500} [Mpc]	kT_X [keV]	σ_{LOS} [km/s]	\mathcal{M}_{vir} [$10^{14} \mathcal{M}_\odot$]	R_{vir} [Mpc]
(1)	(2)	(3)	(4)	(5)	(6)	(7)	(8)	(9)	(10)
A2798B	9.37734	-28.52947	0.1119	60	0.7476	3.39	757	6.01	1.75
A2801	9.62877	-29.08160	0.1122	35	...	3.20	699	6.94	1.83
A2804	9.90754	-28.90620	0.1123	48	...	1.00	516	3.11	1.40
A0085A	10.46052	-9.30304	0.0553	318	1.2103	7.23	1034	19.75	2.65
A2811B	10.53718	-28.53577	0.1078	103	1.0355	5.89	947	13.94	2.32
A0118	13.75309	-26.36238	0.1144	72	680	6.16	1.76
A0119	14.06709	-1.25549	0.0444	294	0.9413	5.82	853	9.51	2.08
A0122	14.34534	-26.28134	0.1136	28	0.8165	3.70	677	4.98	1.64
A0133A	15.67405	-21.88215	0.0562	86	0.9379	4.25	778	7.30	1.90
A2877-70	17.48166	-45.93122	0.0238	112	0.6249	3.28	679	4.20	1.60
AM0227-334	37.33891	-33.53196	0.0780	30	625	4.11	1.56
A3027A	37.70601	-33.10375	0.0784	82	0.7200	3.12	713	7.52	1.90
A0400	44.42316	6.02700	0.0232	51	0.6505	2.25	343	0.68	0.87
A0399	44.47120	13.03080	0.0705	69	1.1169	6.69	950	11.65	2.21
A0401	44.74091	13.58287	0.0736	114	1.2421	7.06	1026	15.11	2.41
A3094A	47.85423	-26.93122	0.0685	84	0.6907	3.15	637	4.83	1.65
A3095	48.11077	-27.14017	0.0652	21	327	0.65	0.84
A3104	48.59055	-45.42024	0.0723	28	0.8662	3.56	498	1.77	1.18
S0334	49.08556	-45.12110	0.0746	26	534	2.11	1.25
S0336	49.45997	-44.80069	0.0773	32	538	3.02	1.40
A3112B	49.49025	-44.23821	0.0756	74	1.1288	5.49	705	8.45	1.98
A0426A	49.95098	41.51168	0.0176	314	1.2856	6.42	1029	13.50	2.36
S0373	54.62118	-35.45074	0.0049	98	0.4017	1.56	390	0.43	0.75
A3158	55.72063	-53.63130	0.0592	249	1.0667	5.42	1066	13.93	2.35
A0496	68.40767	-13.26196	0.0331	279	0.9974	4.64	712	6.31	1.82
A0539	79.15555	6.44092	0.0288	92	0.7773	3.04	698	3.92	1.56
A3391	96.58521	-53.69330	0.0560	75	0.8978	5.89	817	7.74	1.94
A3395	96.90105	-54.44936	0.0496	199	0.9298	5.10	746	6.42	1.82
A0576	110.37600	55.76158	0.0379	191	0.8291	4.27	866	11.18	2.20
A0634	123.93686	58.32109	0.0268	70	395	1.13	1.03
A0754	137.13495	-9.62974	0.0542	333	1.1439	8.93	820	9.10	2.05
A1060	159.17796	-27.52858	0.0123	343	0.7015	2.79	678	3.99	1.57
A1367	176.00905	19.94982	0.0215	226	0.9032	3.81	597	3.76	1.54
A3526A	192.20392	-41.31167	0.0100	126	0.8260	3.40	564	2.43	1.34
A3526B	192.51645	-41.38207	0.0155	45	317	0.44	0.75
A3530	193.90001	-30.34749	0.0536	94	0.8043	3.62	631	4.63	1.63
A1644	194.29825	-17.40958	0.0470	288	0.9944	5.25	1008	13.98	2.36
A3532	194.34134	-30.36348	0.0557	58	0.9201	4.63	443	1.66	1.16
A1650	194.67290	-1.76139	0.0842	146	1.1015	5.72	723	7.55	1.90
A1651	194.84383	-4.19612	0.0849	158	1.1252	7.47	876	12.48	2.25
A1656	194.89879	27.95939	0.0233	919	1.1378	7.41	995	15.66	2.47
A3556	201.02789	-31.66996	0.0482	90	...	3.08	520	2.59	1.35
A1736A	201.68378	-27.43940	0.0350	36	0.9694	3.34	386	1.30	1.08
A1736B	201.86685	-27.32468	0.0456	126	844	8.82	2.03
A3558	201.98702	-31.49547	0.0483	469	1.1010	5.83	955	15.75	2.46
SC1329-313	202.86470	-31.82058	0.0448	46	383	1.01	0.99
A3562	203.39475	-31.67227	0.0486	82	0.9265	5.10	594	3.94	1.55
A1795	207.21880	26.59301	0.0630	154	1.2236	6.42	780	7.09	1.88
A2029	227.73377	5.74491	0.0769	155	1.3344	8.45	931	7.82	1.93
A2040B	228.19782	7.43426	0.0451	104	...	2.41	627	4.77	1.65

TABLE 1 — *continued*

Name ^a	Optical data				X-ray data ^b		Basic properties		
	RA _{CDG} [deg] _{J2000}	Dec _{CDG} [deg] _{J2000}	\bar{z}	N_a	r_{500} [Mpc]	kT_X [keV]	σ_{LOS} [km/s]	\mathcal{M}_{vir} [$10^{14}M_\odot$]	R_{vir} [Mpc]
(1)	(2)	(3)	(4)	(5)	(6)	(7)	(8)	(9)	(10)
A2052	229.18536	7.02167	0.0347	120	0.9465	2.88	648	4.28	1.60
MKW03S	230.46613	7.70888	0.0443	75	607	3.46	1.49
A2065	230.62053	27.71228	0.0730	168	1.0480	6.59	1043	17.01	2.50
A2063A	230.77210	8.60918	0.0345	142	0.9020	3.34	762	6.18	1.81
A2142	239.58345	27.23335	0.0902	157	1.3803	11.63	828	11.06	2.16
A2147	240.57086	15.97451	0.0363	397	0.9351	4.26	935	15.70	2.47
A2151	241.28754	17.72997	0.0364	276	0.7652	2.10	768	8.35	2.00
A2152	241.37175	16.43579	0.0443	64	0.5783	2.41	406	1.56	1.14
A2197	246.92114	40.92690	0.0304	185	0.5093	2.21	573	4.21	1.59
A2199	247.15949	39.55138	0.0303	459	1.0040	4.04	779	7.21	1.91
A2204A	248.19540	5.57583	0.1518	38	1.3998	10.24	1101	20.33	2.59
A2244	255.67697	34.06010	0.0993	102	1.1295	5.99	1161	18.35	2.55
A2256	256.11353	78.64056	0.0586	280	1.1224	8.23	1222	20.63	2.68
A2255	258.11981	64.06070	0.0805	179	1.0678	7.01	1000	16.44	2.47
A3716	312.98715	-52.62983	0.0451	123	...	2.19	783	6.99	1.88
S0906	313.18958	-52.16440	0.0482	26	440	1.46	1.11
A4012A	352.96231	-34.05553	0.0542	39	575	3.15	1.44
A2634	354.62244	27.03130	0.0309	166	0.7458	3.71	717	5.87	1.78
A4038A-49	356.93768	-28.14071	0.0296	180	0.8863	2.84	753	5.95	1.79
A2670	358.55713	-10.41900	0.0760	251	0.9113	4.45	970	9.91	2.09

^a A capital letter after the ACO name indicates the line-of-sight component of the cluster.

^b Taken from Caretta et al. (2023) and references therein.

Columns 2, 3 and 4 present their right ascension, declination and mean redshift coordinates, respectively; Column 5 presents the number of presumably virialized sampled galaxies belonging to the system (inside the caustics and the aperture $1.3 \times r_{200}$); Column 6 presents the radius r_{500} at which the mean interior overdensity is 500 times the critical density at the corresponding redshift; and Column 7 presents the X-ray temperature of clusters.

For each observed cluster, the virial mass was estimated using (3) and the virial radius by

$$R_{vir}^3 = \frac{3\mathcal{M}_{vir}}{4\pi\rho_{vir}} = \frac{\alpha\sigma_{LOS}^2 R_p}{18\pi H^2(z)}. \quad (13)$$

where $\rho_{vir} = 18\pi^2[3H^2(z)/8\pi G]$ is the virialization density assuming a spherical model for nonlinear collapse (*e.g.*, Bryan & Norman 1998). In all calculations we used $\alpha = 2.5$, assuming a weak anisotropy (*e.g.*, Tully 2015; Kashibadze et al. 2020). The line-of-sight velocity dispersions were computed using the Tukey’s biweight robust estimator (Beers et al. 1990). The results of σ_{LOS} , \mathcal{M}_{vir} and R_{vir} are shown, respectively, in Columns 8, 9 and 10 of Table 1.

4.2. Simulation data

In addition, we use data from the IllustrisTNG simulation (*e.g.*, Springel et al. 2018; Nelson et al. 2019), a set of cosmological simulations

that assume initial conditions consistent with the Planck Collaboration (2016) results and take into account magnetohydrodynamical effects. In particular, we use the TNG300-1 data cube that contemplates the largest volume allowing the study of the distribution of galaxies and massive objects such as clusters. We take halos (equivalent to galaxy clusters) from the TNG300-1 simulation at redshift $z = 0$,⁴ which has a resolution of 2500^3 dark matter particles and 2500^3 baryonic matter particles. We sampled 248 halos with masses greater than $10^{14}h^{-1}M_\odot$ with 370,119 member subhalos, of which 366,940 are classified as galaxies. Information related to the peculiar velocity, mass and position of the center of each halo and subhalo was extracted.

Each halo in the simulation contains, on average, 1,300 subhalos within its virial radius, greatly outnumbering the tracers (galaxies) in our observational sample of clusters. This large difference is due to the number of low-mass systems (dwarf galaxies subhalos) entering the count of TNG300-1; these galaxies are hard to detect in real clusters due to their low luminosity. Thus, to avoid statistical differences between the parameters estimated from observational and simulated data, we limit the selection of mem-

⁴The positions are given in rectangular coordinates of the form $(x, y, z) ah^{-1}$ kpc, where a is the cosmological scale factor, being $a = 1$ in $z = 0$, and $h = H_0/(100 \text{ km s}^{-1} \text{ Mpc}^{-1})$, for which a value of $h = 0.7$ was assumed here.

ber subhalos by taking only those with mass greater than $2.0 \times 10^{10} h^{-1} \mathcal{M}_{\odot}$. For each halo, all member subhalos up to a distance of $1.3 \times r_{200}$ from the center (the particle with the least gravitational potential energy) were taken. Also, σ_{LOS} , \mathcal{M}_{vir} and R_{vir} were calculated reproducing the observational procedure.

Fig. 1 shows the projected distribution of member subhalos for two halos in the sample, one high-entropy (left) and one low-entropy (right). Note that, as expected, the distribution of subhalos is more random and homogeneous in a high entropy halo, while more substructured and elongated in a low entropy halo. This also happens in the observed clusters, reinforcing our hypothesis that evolutionary changes in galaxy systems progress in the direction in which the system dissolves substructures, becoming observationally more regular and homogeneous, with higher entropy values.

4.3. Results on the assembly state of observed clusters

To appreciate the correlation between the H_Z entropy (shown in Column 3 of Table 2 below) and the gravitational assembly level—and therefore with the evolutionary state—of galaxy systems, we present in Fig. 2 the distributions of the H_Z values with respect to the assembly state classes. These are displayed in the form of boxplots, which allow graphically describing the locality, dispersion and asymmetry of data classes (groups) of a quantitative variable through its quartiles (*e.g.*, Heumann & Shalabh 2016). The classes were ordered from more to less relaxed systems. Although the box overlap does not allow one to unambiguously discriminate the class to which an arbitrary individual cluster should belong, the statistical correlation is clear: the sequence U-P-S-M-L follows directly the decreasing median values of entropy. The only marginal difference case is between U and P systems, which is understandable if we consider that the primary systems (with only low significance substructures) are dynamically very similar to the unimodal ones—both tend to be relatively massive and evolved systems. This discussion will be resumed later.

5. TESTING STATISTICALLY THE H_Z -ENTROPY ESTIMATOR

5.1. Shannon entropy of galaxy distributions in phase-spaces

Another way we use to evaluate the entropy estimates that H_Z can provide is by using a method that does not take into account equilibrium assumptions, but allows to characterize the internal states

of a galaxy system from the raw distribution of its member galaxies. In information theory, for example, entropy is a measure of the uncertainty of a random variable (or source of information, *e.g.*, Shannon 1948; Cover & Thomas 2006). If X is a discrete random variable with possible observable values $x \in \mathcal{X}$, which occur with probability $p(x) = \Pr\{X = x\}$, the Shannon (or information) entropy of X is defined as

$$H_S(X) \equiv - \sum_{x \in \mathcal{X}} p(x) \log_{\lambda} p(x), \quad (14)$$

where the sum is performed over all possible values of the variable, and the base λ of the logarithm is chosen according to the entropy ‘units’ to use (*nats*, $\lambda = e$; *bits*, $\lambda = 2$; *bans*, $\lambda = 10$). One of the criteria used by Shannon (1948) to define H_S ensures that it increases as the possible values of X begin to appear with equal frequency, taking higher values when they become equiprobable, *i.e.*, when there are no special configurations in the data distribution that provide more information, increasing the uncertainty.

Now, the raw coordinates of the galaxies in a cluster, *i.e.* the observable set of triples (RA, Dec, z) of right ascension, declination and redshift, are distributed within a solid angle, which can be approximated by a cylinder with a circular base in the plane of sky and depth along the line-of-sight (see, Fig. 3, left panel). Inside the cylinder, the position of each galaxy can be expressed in the form $x = (r, \theta, z)$, where r is its projected distance from the cluster center, θ its—azimuthal—angle with respect to the local north direction in the projected sky distribution (see, Fig. 3, right panel), and the redshift z a measure of its radial velocity. In fact, the cylinder of x -coordinates (two spatial and one velocity) may be considered a—projected—phase-space for the galaxy ensemble, and the distribution of the variables (r, θ, z) inside it depend on the dynamical state of the galaxy cluster.

By considering the cylinder of sampled galaxies as a source of information for the x -distribution, the probability of finding a galaxy in the neighborhood of position x (*i.e.*, the probability that the position random variable X takes a value very close to x inside the cylinder) can be approximated as $p(x) \simeq \bar{f}_{r\theta z}(x) \Delta x$, where $\bar{f}_{r\theta z}$ must be the observed—or empirical—joint probability density function (PDF) that represents the actual distribution of the galaxy ensemble in the variable x . Replacing this in (14), one can compute the Shannon entropy of the

TABLE 2
DYNAMICAL PARAMETERS FOR TOP70 CLUSTER SAMPLE.

Name	\mathcal{A}^a	H_Z	H_S [nat]	r'_c [Mpc]	$\mathcal{P}_{\text{relax}}$	c_K	c_{NFW}	c_{ICM}
(1)	(2)	(3)	(4)	(5)	(6)	(7)	(8)	(9)
A2798B	U	15.54	10.85	0.28	0.808	7.85	3.91	2.33
A2801	U	15.34	10.60	0.29	0.794	3.94	1.22	...
A2804	M	14.58	10.16	0.22	0.668	3.41	1.55	...
A0085A	S	16.26	12.48	0.42	0.816	4.76	1.89	2.18
A2811B	S	16.09	11.69	0.37	0.762	5.42	1.77	2.23
A0118	S	15.27	11.25	0.28	0.680	1.76	1.17	...
A0119	S	15.77	11.90	0.33	0.893	7.00	3.88	2.21
A0122	U	15.26	10.72	0.26	0.839	8.29	5.03	2.00
A0133A	S	15.55	11.26	0.30	0.792	7.10	3.36	2.02
A2877-70	S	15.18	10.99	0.25	0.828	10.59	6.95	2.55
AM0227-334	L	15.03	9.36	0.25	0.650	3.72	1.97	...
A3027A	S	15.36	11.20	0.30	0.825	3.32	1.26	2.64
A0400	S	13.47	8.65	0.14	0.816	7.32	3.46	1.33
A0399	U	16.07	12.03	0.35	0.775	6.43	4.61	1.97
A0401	U	16.26	12.25	0.38	0.841	8.86	5.43	1.93
A3094A	U	15.06	11.13	0.26	0.865	3.93	1.28	2.38
A3095	L	13.39	7.66	0.13	0.645	1.95	0.56	...
A3104	S	14.45	9.54	0.19	0.704	7.52	4.44	1.35
S0334	L	14.63	9.77	0.20	0.757	12.41	7.42	...
S0336	L	14.65	9.39	0.22	0.730	4.84	1.38	...
A3112B	S	15.33	11.11	0.32	0.756	1.98	1.32	1.75
A0426A	P	16.22	12.48	0.38	0.824	11.44	7.29	1.83
S0373	S	13.78	9.13	0.12	0.823	6.11	2.58	1.86
A3158	S	16.34	12.28	0.37	0.761	10.73	8.35	2.20
A0496	S	15.31	11.54	0.29	0.919	6.26	2.99	1.82
A0539	S	15.26	10.91	0.25	0.814	10.51	5.45	2.00
A3391	U	15.67	11.38	0.31	0.804	9.75	5.43	2.15
A3395	M	15.44	11.50	0.29	0.781	6.67	3.64	1.96
A0576	S	15.80	11.98	0.35	0.830	6.26	2.93	2.65
A0634	L	13.83	9.31	0.16	0.746	2.41	0.68	...
A0754	M	15.68	12.07	0.33	0.836	4.88	2.04	1.78
A1060	P	15.17	11.29	0.25	0.874	9.76	6.62	2.24
A1367	M	14.86	10.64	0.24	0.848	4.10	1.61	1.70
A3526A	P	14.71	10.33	0.21	0.823	8.40	4.62	1.61
A3526B	S	13.27	7.57	0.12	0.725	4.26	1.16	...
A3530	S	15.03	11.07	0.26	0.888	5.42	2.24	2.02
A1644	P	16.19	12.39	0.38	0.838	7.51	5.26	2.37
A3532	S	14.14	9.75	0.18	0.778	3.59	1.19	1.26
A1650	U	15.40	11.32	0.30	0.846	3.42	1.26	1.72
A1651	P	15.88	11.97	0.36	0.833	4.42	1.67	1.99
A1656	S	16.14	12.73	0.39	0.861	7.79	4.11	2.17
A3556	M	14.54	10.85	0.21	0.744	3.79	1.49	...
A1736A	S	13.78	9.34	0.17	0.783	2.75	0.71	1.10
A1736B	S	15.75	11.77	0.32	0.775	5.74	3.64	...
A3558	P	16.06	12.60	0.39	0.826	4.89	2.12	2.23
SC1329-313	L	13.77	8.65	0.16	0.744	4.63	2.34	...
A3562	U	14.87	10.70	0.25	0.841	4.15	1.74	1.67
A1795	U	15.56	11.51	0.30	0.893	9.47	5.04	1.53
A2029	U	16.02	11.81	0.31	0.838	12.94	6.92	1.44
A2040B	S	15.00	10.76	0.26	0.838	4.28	1.10	...

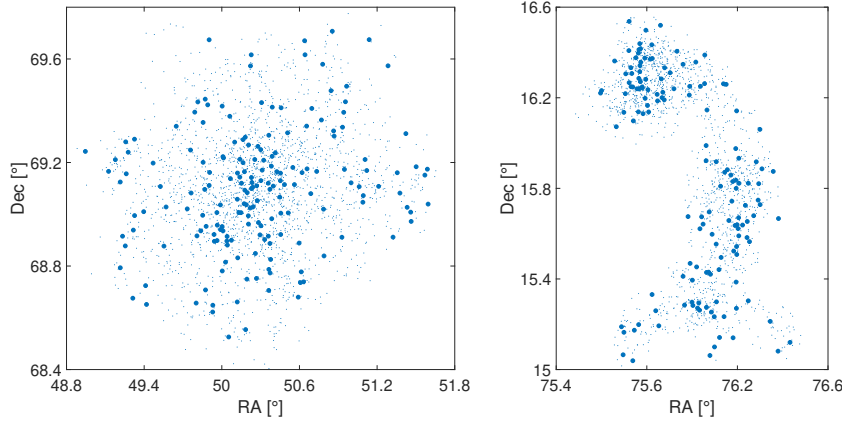


Fig. 1. Two examples of sampled TNG300 halos. *Left*: subhalo distribution for a high entropy halo (TNG-halo-34). *Right*: subhalo distribution for a low entropy halo (TNG-halo-87). Each dot represents a member subhalo: the small dots are subhalos with masses less than $2.0 \times 10^{10} M_{\odot}$ while the big dots are the subhalos taken for our analysis.

TABLE 2 — *continued*

Name	\mathcal{A}^a	H_Z	H_S	r'_c	$\mathcal{P}_{\text{relax}}$	c_K	c_{NFW}	c_{ICM}
(1)	(2)	(3)	[nat] (4)	[Mpc] (5)	(6)	(7)	(8)	(9)
A2052	S	15.08	10.98	0.25	0.850	6.82	3.69	1.69
MKW03S	U	14.92	11.30	0.24	0.881	6.58	4.01	...
A2065	U	16.30	12.19	0.40	0.882	9.11	5.24	2.38
A2063A	P	15.48	11.50	0.29	0.899	9.51	5.19	2.00
A2142	P	15.74	12.12	0.34	0.866	4.54	1.82	1.56
A2147	M	15.99	12.00	0.39	0.829	3.62	1.64	2.63
A2151	M	15.50	11.85	0.32	0.823	4.18	1.36	2.61
A2152	M	13.91	9.38	0.18	0.758	1.99	0.75	1.96
A2197	M	14.76	10.65	0.25	0.699	1.59	1.06	3.12
A2199	P	15.53	12.02	0.30	0.884	7.41	4.23	1.89
A2204A	S	16.51	11.16	0.41	0.769	3.92	1.72	1.84
A2244	U	16.60	12.33	0.41	0.821	10.46	7.81	2.25
A2256	S	16.68	12.47	0.43	0.607	10.87	8.49	2.39
A2255	S	16.20	12.31	0.39	0.789	6.54	3.42	2.31
A3716	M	15.56	11.56	0.30	0.769	5.53	3.17	...
S0906	L	14.12	9.30	0.18	0.793	2.94	0.74	...
A4012A	L	14.80	10.13	0.23	0.834	4.26	1.63	...
A2634	S	15.32	11.60	0.28	0.861	6.69	3.81	2.38
A4038A-49	S	15.45	11.35	0.28	0.820	9.73	5.12	2.01
A2670	U	16.12	11.92	0.33	0.859	10.24	6.01	2.29

^a Gravitational assembly classes from Caretta et al. (2023).

galaxy distribution for a cluster in the form

$$H_S = - \sum_{x \in \mathcal{X}} [f_{r\theta z}(x) \Delta x] \ln \{ f_{r\theta z}(x) \Delta x \}, \quad (15)$$

where $\lambda = e$ has been chosen, and the sum is performed over all the n discrete partitions Δx made to the domain $\mathcal{X} = [0, R_{\text{vir}}] \times [0, 360] \times [z_{\text{min}}, z_{\text{max}}]$ of the observed joint PDF. Here, z_{min} and z_{max} are the minimum and maximum values of redshift in the sample of galaxies of each cluster.

Shannon entropy is a well-established measure for quantifying disorder or uncertainty in a system (*e.g.*, Cover & Thomas 2006). In this context, H_S provides a measure of the degree of randomness in the distribution of galaxies in the phase-space of a cluster (or any other galaxy system). By calculating this entropy, we are evaluating the information contained in the galaxy ensemble and how galaxies are distributed in different regions of phase-space. Close to equilibrium, the memory (information) of the initial conditions of clusters formation is lost

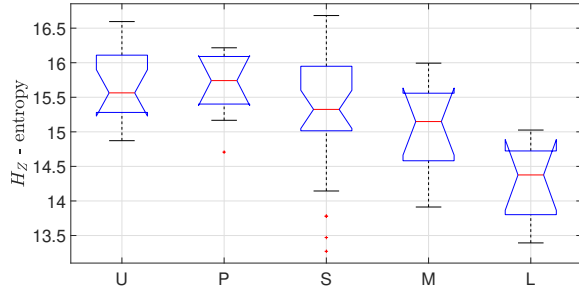


Fig. 2. Boxplots of H_Z -entropy for the five assembly classifications of clusters. The lower and upper extremes of each box are the 25th and 75th percentiles, respectively, while the central red line marks the median. Whiskers extend to the most extreme non-outlier data, while outliers are represented by red ‘+’ symbols.

(*e.g.*, Binney & Tremaine 2008; Araya-Melo et al. 2009). The general character of H_S comes from the fact that it is not restricted only to thermodynamic variables, but to any type of data X that contains information about the state of a system, so it can be used to study characteristics of non-equilibrium systems as they evolve. In addition, it does not consider the microstates of a system as equiprobable, keeping a certain relationship in mathematical form and meaning with the Gibbs entropy (*e.g.*, Jaynes 1957).

5.2. Shannon entropy estimations

To calculate the Shannon entropy, we first established the observed joint PDF $\bar{f}_{r\theta z}(x)$ of each cluster in two different ways. First, by counting galaxies independently in bins of width Δr , $\Delta\theta$ and Δz in the radial- r , azimuthal- θ and redshift- z directions, respectively, we constructed 1D-histograms that describe the observed distribution of that variables in the galaxy ensemble. Then, by a smoothing technique, the *observed PDFs* $\bar{f}_r(r)$, $\bar{f}_\theta(\theta)$ and $\bar{f}_z(z)$ were obtained for the variables from their respective normalized histograms (see, red solid lines on graphs in Fig. 4). For this, we used a kernel density estimator that allows a non-parametric fit of PDFs of random variables, adapting directly to the data (*e.g.*, Heumann & Shalabh 2016). This method is particularly useful when the actual distribution of a data set is unknown, as is the case for the galaxy distributions inside the (phase-space) cylinders. A standard Gaussian smoothing kernel was used with bins of widths $\Delta r = 0.15$ Mpc, $\Delta\theta = 12^\circ$, $c\Delta z = 200$ km s $^{-1}$ and supports in

the intervals $[0, R_{\text{vir}}]$, $[0, 360]$ and $[z_{\text{min}}, z_{\text{max}}]$ for the \bar{f}_r , \bar{f}_θ and \bar{f}_z distributions, respectively. Finally, we took $\bar{f}_{r\theta z}(r, \theta, z) = \bar{f}_r(r)\bar{f}_\theta(\theta)\bar{f}_z(z)$ assuming statistical independence of the variables r , θ and z in the galaxy distributions.

On the other hand, as is evident in the right panel of Fig. 3, galaxies with the highest and lowest redshifts prefer the center of the projected distribution of the cluster. This correlation between the variables r and z is physically justified since the galaxies acquire a greater speed during their transit through the central regions of the clusters (*i.e.*, where the gravitational potential well is the deepest). Projection effects can also occur, especially for halo galaxies that are located in front or behind the core and close to the line-of-sight. No significant correlation was detected between the variables r or z with θ instead. Thus, to construct the observed joint PDF in the second way we only took into account the correlation between r and z , such that $\bar{f}'_{r\theta z}(r, \theta, z) = \bar{f}'_{rz}(r, z)\bar{f}_\theta(\theta)$, where the \bar{f}'_{rz} functions were obtained by counting galaxies in bi-dimensional bins of “area” $\Delta r\Delta z$ and smoothed by a multivariate Gaussian surface kernel, using the same bin width values as above.

Two statistical tests, Kolmogorov-Smirnov and Rank-Sum, showed no significant differences between both methods, confirming the null hypothesis that the PDFs $\bar{f}_{r\theta z}$ and $\bar{f}'_{r\theta z}$ represent the same distribution with a confidence level of 95% in both tests. This is probably because the fraction of galaxies that present a strong rz -correlation is very small, implying a low statistical weight. Then, for simplicity we choose the first option (*i.e.*, that with the three variables assumed to be statistically independent, see Fig. 4) to compute the probability values

$$p(x) \simeq \bar{f}_{r\theta z}(x)\Delta x = [\bar{f}_r(r)\Delta r][\bar{f}_\theta(\theta)\Delta\theta][\bar{f}_z(z)\Delta z], \quad (16)$$

varying one of the variables in its respective domain (*e.g.*, $r \in [0, R_{\text{vir}}]$, $\theta \in [0, 360]$ and $z \in [z_{\text{min}}, z_{\text{max}}]$), while keeping the other two constant. Thus, $p(x)$ was obtained in about 1,000 positions $x = (r, \theta, z)$ inside the data cylinder of each real (and simulated) cluster and these values were used to compute the respective H_S -entropies by (15) for the galaxy ensembles. The results for *Top70* clusters are shown in Column 4 of Table 2.

5.3. Results on the Shannon entropy for observed and simulated clusters

The relation between the H_Z -entropy estimator, proposed in the present work, and the Shannon entropy H_S of the real galaxy distributions can be seen

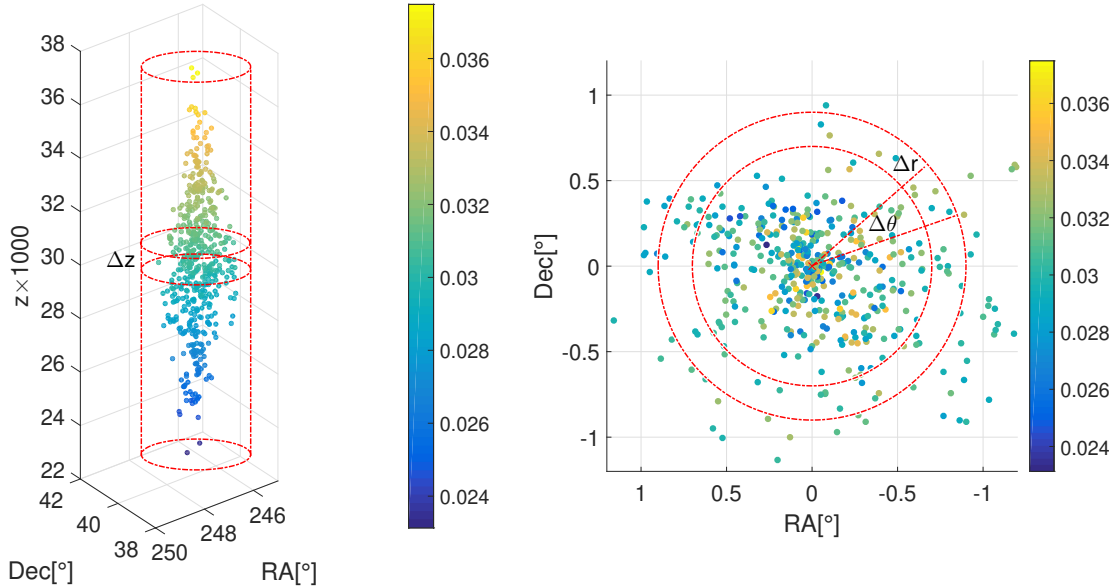


Fig. 3. Sample of galaxies for A2199 cluster in Caretta et al. (2023). Color bars represent the redshift (z) distribution. *Left panel*: the cylinder along the line-of-sight direction. *Right panel*: projected distribution in the sky plane with RA and Dec coordinates transported to the origin (the FRG, see the text).

in Fig. 5, where the dashed line represents the best fit curve, with a coefficient of determination (\mathcal{R}^2 , *e.g.*, Heumann & Shalabh 2016) of 0.886. This figure shows a high degree of correlation (almost linear) between H_Z and H_S entropies that, when measured by the Pearson and Spearman coefficients (*e.g.*, Gibbons & Chakraborti 2003; Heumann & Shalabh 2016), gives the values 0.932 and 0.922, respectively. Below (see, section 7), we offer what we believe to be a possible explanation for such an explicit correlation. In addition, the figure also shows the association of these H_Z and H_S entropy values with the assembly state of the clusters (represented by the U-P-S-M-L classes). Although the correlation is not evident, it is noticeable that all U and P clusters are placed in the locus of points with higher values of both H_Z and H_S , while all L are located in the region with lower values of these entropies.

A procedure similar to that performed with *Top70* clusters was applied to the TNG300 sample to compare the H_Z and H_S entropies estimated for the simulated halos. Fig. 6 shows a significant correlation, with Pearson and Spearman coefficients of 0.709 and 0.678, respectively, between the dynamical and Shannon entropies, which reveal to be very similar to that of real clusters. We did not carry out a classification of simulated clusters in their different assembly levels (\mathcal{A}) that allows us to analyze the distribution of H_Z in each class, as

in the case of real clusters. We hope to do this in future work.

6. OTHER VALIDATIONS FOR H_Z

6.1. The relaxation probability of galaxy systems

Several studies reveal that clusters close to dynamical equilibrium have distributions of galaxies whose radial density and LOS velocity profiles tend to ones that can be represented by specific mathematical functions (*e.g.*, Saslaw & Hamilton 1984; Sarazin 1988; Adami et al. 1998; Sampaio & Ribeiro 2014). The above is also true for the ICM entropy profiles in X-ray observations (*e.g.*, Voit 2005) or for the distribution of DM subhalos in cosmological simulations (*e.g.*, Navarro, Frenk & White 1996). Thus, we consider that it is also possible to characterize the evolutionary state of a galaxy system by measuring how far the currently *observed PDFs* are from their expected equilibrium functional shapes. For this, we need to use (or choose) a consistent reference equilibrium model that describes the distribution when the galaxy ensemble is relaxed, as well as a metric that allows us to estimate the distance of the observed distribution from that of the equilibrium model.

We limit ourselves to a simple reference equilibrium model, considering clusters represented by a spherical distribution of galaxies, with a homogeneous core-halo spatial configuration and an

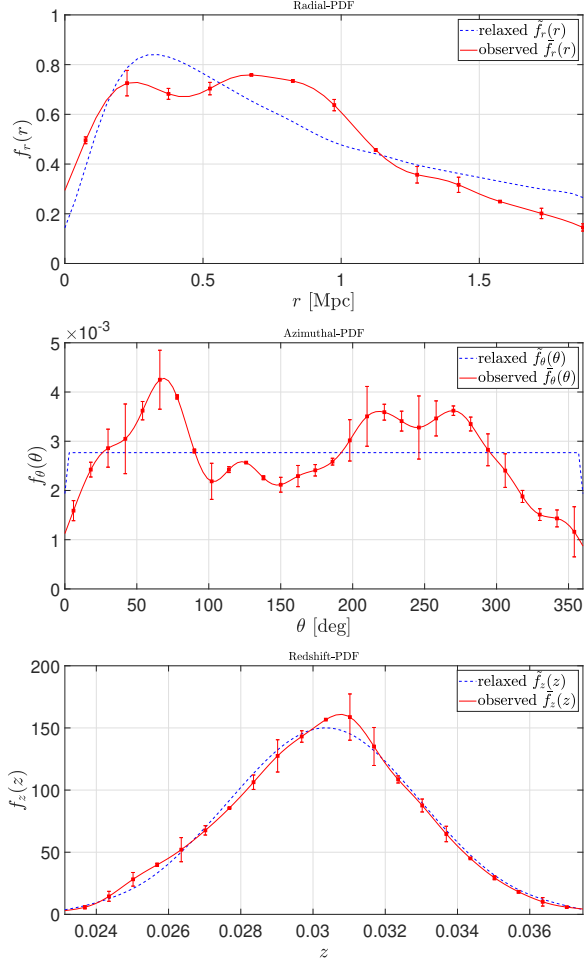


Fig. 4. Probability density functions for the radial- r , azimuthal- θ and redshift- z distributions of member galaxies in the A2199 cluster. The red solid lines represent the *observed PDFs* obtained by smoothing (normal kernel) from observational data histograms, while dashed blue lines represent the *relaxed PDFs* of equilibrium distributions. The error bars represent the difference between the height of the smoothed curve and the height of the corresponding bin in each 1D-histogram.

isotropic velocity distribution without net angular momentum.

In principle, the radial distribution of galaxies can be well described (see, Adami et al. 1998) by different single popular mass profiles proposed for clusters in the literature, both *core-* (e.g., King, Einasto; respectively King 1962; Einasto 1965) and *cuspy-* (e.g., Hernquist, NFW, respectively Hernquist 1990; Navarro, Frenk & White 1996) dominated ones. Nonetheless, there has been a tendency, especially for fitting DM halos, to use more complex functions, with a larger number of free

parameters (e.g., Dehnen 1993; Fielder et al. 2020; Diemer 2023) –although they are essentially double and/or truncated power laws–, in order to better accommodate the inner and outer slopes. On the other hand, since *core-*dominated profiles usually perform slightly better for real clusters (e.g., Sarazin 1988; Adami et al. 1998; García-Manzanárez 2022) –as commented before, the core-halo structure is the one expected for self-gravitating systems at equilibrium– and considering the simplest as possible analytical form, we choose the King density profile at this point. Such profile can be approximated analytically by the form

$$\rho(r) = \rho_0 \left[1 + \left(\frac{r}{r_c} \right)^2 \right]^{-\gamma}, \quad (17)$$

suggesting a finite central density $\rho_0 = \rho(0)$ and the existence of a core of radius r_c . The parameters r_c , ρ_0 and γ can be determined by the best fit of the model (17) to the spatial distribution of galaxies. For three-dimensional distributions it has been found that $\gamma = 3/2$ and $\rho_0 = 9\sigma_{LOS}^2/4\pi Gr_c^2$, while for observed two-dimensional (or projected) distributions $\gamma = 1$ and $\rho_0 = 9\sigma_{LOS}^2/2\pi Gr_c$ (see, Rood et al. 1972; Schneider 2015), where G is the gravitational constant. Thus, here we consider the projection (on the RA-Dec plane) of a cluster in equilibrium to have a King-type radial distribution of galaxies described by the (1D) radial-PDF of the form

$$f_r^{\text{eq}}(r) = \frac{6r}{\pi r_c' R_{\text{vir}}} \left[1 + \left(\frac{r}{r_c'} \right)^2 \right]^{-1}, \quad (18)$$

in which the count of galaxies must be performed in bins of length Δr instead of rings of area $\Delta A = 2\pi r \Delta r$, that is, counting the number of galaxies located between r and $r + \Delta r$ for each distance from the cluster center. Integrating (18) from 0 to R_{vir} , the normalization condition to find the ‘relaxed’ core radius (r_c') in virial equilibrium is

$$\ln \left(1 + \frac{R_{\text{vir}}^2}{r_c'^2} \right) = \frac{\pi R_{\text{vir}}}{3r_c'}. \quad (19)$$

For the azimuthal distribution of galaxies on the RA-Dec projected plane of a regular cluster we expect a continuous uniform azimuthal-PDF of the form

$$f_{\theta}^{\text{eq}}(\theta) = \begin{cases} 1/360, & \text{for } \theta \in [0, 360] \\ 0, & \text{otherwise,} \end{cases} \quad (20)$$

since, under the assumed equilibrium model, the probability of finding galaxies in any direction of the

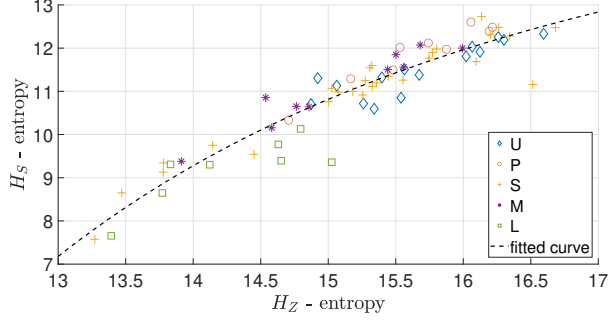


Fig. 5. Scatter plot of H_Z vs. H_S made with the entropy values estimated for the *Top70* clusters. The symbols and color scale of the points represents the U-P-S-M-L assembly level classification of clusters performed by Caretta et al. (2023). The dashed line represents the best —power law— fit with $\mathcal{R}^2 = 0.886$.

plane must be the same if there are no deformities (flattening or elongation) in the cluster morphology and no substructures when counting galaxies in slices of width $\Delta\theta$ at fixed radius.

Finally, for the (3D) galaxy velocities inside clusters in equilibrium we expect a quasi-Maxwellian distribution (isotropic, *e.g.*, Sarazin 1988; Sampaio & Ribeiro 2014), so that the LOS component of velocities have a normal distribution described by the redshift-PDF

$$f_z^{\text{eq}}(z) = \frac{c}{\sigma_{LOS}\sqrt{2\pi}} \exp\left\{-\frac{c^2}{2}\left(\frac{z-\bar{z}}{\sigma_{LOS}}\right)^2\right\}, \quad (21)$$

where c is the speed of light and $c\bar{z}$ is the mean LOS velocity of the cluster.

The construction of the reference PDFs associated to the data is done in three steps. First, we determine numerically the relaxed core radius r'_c (see, Column 5 of Table 2 for observational sample), taking into account the normalization condition (19), to be used in f_r^{eq} . For R_{vir} , also used in f_r^{eq} , and for $c\bar{z}$ and σ_{LOS} , the last ones for f_z^{eq} , we take the previously calculated parameters (see, Columns 10, 4 and 8, respectively, of Table 1 for observational sample). The f_θ^{eq} distribution is trivial and does not require observational parameters of clusters.

Next, for each cluster we construct its corresponding relaxed mock cluster, which have as many particles as observed galaxies but distributed according to (or following) the corresponding f_r^{eq} , f_θ^{eq} and f_z^{eq} equilibrium PDFs.

The third step is done by fitting the tuned equilibrium models to the particle distributions of the mock clusters in the radial, azimuthal, and redshift

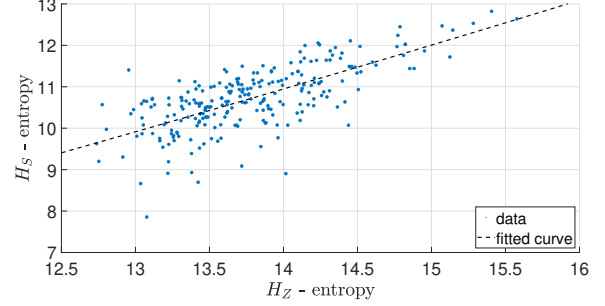


Fig. 6. Scatterplot of H_S vs. H_Z entropies made with the data of the complete TNG300 sample. The dashed line represents the best power law fit with $\mathcal{R}^2 = 0.505$.

components, using bin widths and smoothing levels equal to those used in the *observed PDFs*. With this, we are able to construct the *relaxed PDFs*, \tilde{f}_r , \tilde{f}_θ and \tilde{f}_z , *i.e.*, the ones expected in the dynamical relaxation state. Fig. 4 shows an example of the *observed* and *relaxed PDFs* for the A2199 cluster.

Now, the relaxation probability of a galaxy system can be defined as a distance between the *observed PDFs* and the *relaxed* ones, *i.e.*, between the current dynamical state of the galaxy ensemble (characterized by \tilde{f}_r , \tilde{f}_z and \tilde{f}_θ) and its most probable equilibrium state (characterized by \tilde{f}_r , \tilde{f}_θ and \tilde{f}_z), in the probability space. For this, we use the Hellinger distance (Hellinger 1909), a metric used to quantify the similarity between two distributions in the same probability space so that, if f_1 and f_2 represent two PDFs for the same variable, the Hellinger distance between them is defined as

$$H(f_1, f_2) \equiv \left[\frac{1}{2} \int \left(\sqrt{f_1(x)} - \sqrt{f_2(x)} \right)^2 dx \right]^{1/2}, \quad (22)$$

where the integration must be carried out over the domain of the functions, and the property $0 \leq H(f_1, f_2) \leq 1$ allows us to define the relaxation probability, $\mathcal{P}_{\text{relax}} \equiv 1 - H$, of a galaxy ensemble. Thus, the close the \tilde{f}_i and \tilde{f}_i functions are to each other, the more relaxed a galaxy system can be considered. For a system close to equilibrium $H \rightarrow 0$ and $\mathcal{P}_{\text{relax}} \rightarrow 1$.

Under the same assumption of statistical independence between the variables r , θ and z used for the observed joint PDFs, the relaxed joint PDFs were then defined as $\tilde{f}_{r\theta z}(r, \theta, z) = \tilde{f}_r(r)\tilde{f}_\theta(\theta)\tilde{f}_z(z)$. For calculations of H , we take $f_1 = \tilde{f}_{r\theta z}$ and $f_2 = \tilde{f}_{r\theta z}$ in (22) for each galaxy cluster. The calculated values for relaxation probability, $\mathcal{P}_{\text{relax}}$, for the observed clusters are shown in Column 6 of Table 2.

In addition, the top panel of Fig. 7 shows the

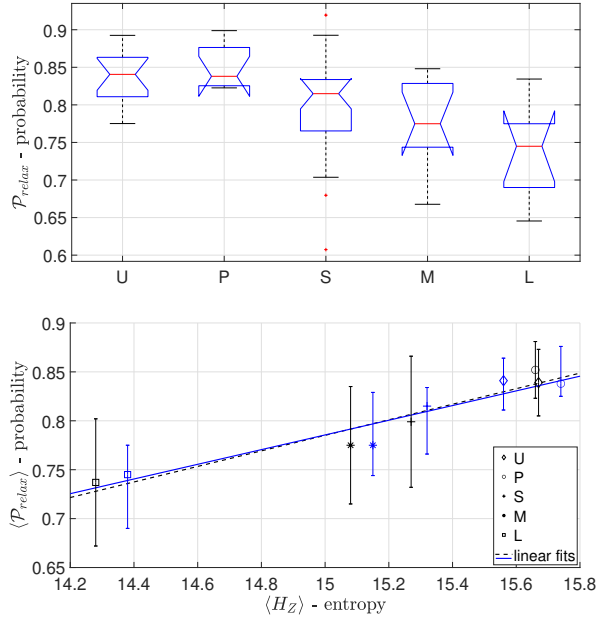


Fig. 7. *Top panel:* Boxplots of $\mathcal{P}_{\text{relax}}$ values for the five assembly states of clusters from Caretta et al. (2023). *Bottom panel:* Scatter plot of $\langle \mathcal{P}_{\text{relax}} \rangle$ vs. $\langle H_Z \rangle$ made with mean (black markers) and median (blue markers) H_Z and $\mathcal{P}_{\text{relax}}$ values presented in Table 3. The symbols of the points represent the U-P-S-M-L assembly level classes. The black dashed and blue solid lines represent the linear fits to the mean and median data, with \mathcal{R}^2 of 0.964 and 0.950, respectively.

distribution of $\mathcal{P}_{\text{relax}}$ values with respect to the assembly state classes. Like what happened with the H_Z -entropy, there is a clear correlation between the relaxation probability and the level of gravitational assembly of a system: the sequence U-P-S-M-L considered here goes from the most likely relaxed to the least relaxed systems with respect to the chosen equilibrium model. The triple correlation between dynamical entropy, the relaxation probability and the assembly level of clusters can be seen in the bottom panel of Fig. 7, a scatterplot of $\langle \mathcal{P}_{\text{relax}} \rangle$ vs. $\langle H_Z \rangle$ built with the mean and median values (see, Table 3) obtained for H_Z and $\mathcal{P}_{\text{relax}}$ in each assembly classification.

Finally, we applied a Kolmogorov-Smirnov (KS-) test to evaluate, with a confidence level set at 90% (or significance level of 0.1), the null hypothesis that the H_Z or $\mathcal{P}_{\text{relax}}$ values for the galaxy systems classified into two different assembly classes (U, P, S, M and L) come from the same continuous distribution. Table 4 shows the p -values, in the range $[0, 1]$, that

resulted from the KS-test. The closer a p -value is to 1, the more similar are the distributions of H_Z and $\mathcal{P}_{\text{relax}}$ values in two different assembly (\mathcal{A}) classes.

6.2. Relation between H_Z and the cluster concentration indices

Apart from the discrete characterization of the assembly state used in the previous sections, one can also probe some continuous parameters, estimated from optical or X-ray data (e.g., Carlberg et al. 1996; Girardi & Mezzetti 2001; Zhang et al. 2011; Caretta et al. 2023, and references therein), that are expected to correlate with the evolutionary state of the galaxy system. Here we present, for instance, the concentration indices of a cluster, both from optical galaxy distributions and X-ray from ICM: more relaxed clusters tend to be denser at their centers and have higher values for these indices.

For the optical data, we use the Maximum Likelihood Estimation method (MLE) to determine the optimal concentration indices for the King and NFW radial profiles fitted to the observed projected distributions of galaxies in the clusters of the *Top70* sample. The King profile employed for the fitting is the one described by equation (17), while the NFW profile takes the form

$$\rho(r) = \rho_0 \left[\left(\frac{r}{r_s} \right) \left(1 + \frac{r}{r_s} \right)^2 \right]^{-\gamma}, \quad (23)$$

where r_s is the scale radius of the galaxy cluster. The concentration indices of each cluster are related to its respective virial and characteristic radii (r_c or r_s obtained by MLE) in the form $c_K = R_{\text{vir}}/r_c$ and $c_{\text{NFW}} = R_{\text{vir}}/r_s$ (e.g. Binney & Tremaine 2008), and the obtained values are compiled in Columns 7 and 8 of Table 2. We also probed the ratio $c_{500} = R_{\text{vir}}/r_{500}$ (using the available X-ray data in Table 1), the obtained values shown in Column 9 of the Table 2.

Figure 8 shows the relationship between the H_Z -entropy and the estimated —cluster— concentration indices for the *Top70* sample. The Pearson correlation coefficients between the H_Z -entropy values and those corresponding to the indices c_K , c_{NFW} and c_{500} are 0.448, 0.512, 0.429, respectively. However, despite the not strong statistical significance and the remarkable dispersion, an evident growing trend can be seen in the concentration indices with the growth of the H_Z -entropy in the systems. This tendency is also subtly manifested in the assemblage classes (represented by the marker symbols in Figure 8): the U and P clusters tend to have higher concentration indices, while the L clusters tend to present

TABLE 3

MEAN (WITH STANDARD DEVIATION) AND MEDIAN (WITH THE FIRST-25% AND THIRD-75% QUANTILES) VALUES FOR H_Z AND $\mathcal{P}_{\text{RELAX}}$ IN EACH OF THE ASSEMBLY STATE CLASSES.

Assembly level class	Mean \pm std		Median $^{+Q3}_{-Q1}$	
	H_Z	$\mathcal{P}_{\text{relax}}$	H_Z	$\mathcal{P}_{\text{relax}}$
U	15.67 ± 0.53	0.839 ± 0.034	$15.56^{+0.55}_{-0.28}$	$0.841^{+0.023}_{-0.030}$
P	15.66 ± 0.50	0.852 ± 0.029	$15.74^{+0.35}_{-0.34}$	$0.838^{+0.038}_{-0.013}$
S	15.27 ± 0.91	0.799 ± 0.067	$15.32^{+0.62}_{-0.31}$	$0.815^{+0.019}_{-0.049}$
M	15.08 ± 0.65	0.775 ± 0.060	$15.15^{+0.41}_{-0.56}$	$0.775^{+0.054}_{-0.031}$
L	14.28 ± 0.58	0.737 ± 0.065	$14.38^{+0.35}_{-0.57}$	$0.745^{+0.030}_{-0.055}$

TABLE 4

P -VALUES OF KOLMOGOROV-SMIRNOV TEST COMPARING THE DISTRIBUTIONS OF H_Z -ENTROPY (LEFT VALUES) AND RELAXATION PROBABILITY $\mathcal{P}_{\text{RELAX}}$ (RIGHT VALUES) FOR GALAXY CLUSTERS IN DIFFERENT CLASSIFICATIONS. THE CONFIDENCE LEVEL FOR THE KS-TEST WAS 90%.

Class	P		S		M		L	
U	0.958	0.500	0.417	0.024	0.065	0.024	2.003e-04	7.725e-04
P	-	-	0.205	0.006	0.203	0.037	7.652e-04	9.766e-04
S	-	-	-	-	0.509	0.714	7.044e-04	0.019
M	-	-	-	-	-	-	0.148	0.243

lower values of these. S and M clusters appear with a more extended range of concentration indices. It is interesting to note that if we leave only U and P clusters in the above relation, for example for c_{500} , the correlation increases from 0.429 to 0.603 —these are the typical clusters that appear in studies based on X-rays emission of ICM.

We have also probed other continuous dynamical parameters, obtained from X-rays emission of ICM, associated to the evolutionary state of galaxy systems: the concentration c and the luminosity concentration c_L (respectively from, Parekh et al. 2015; Zhang et al. 2017), the Gini and M_{20} morphological coefficients (from Parekh et al. 2015; Lovisari et al. 2017), the substructure level S_C (from Andrade-Santos et al. 2012), and the C_{SB} and C_{SB4} concentration parameters (from Andrade-Santos et al. 2017). Although the statistics are usually poor, and the aspects captured from X-ray data are not necessarily similar to the ones captured by optical data (which include H_Z), the results are all similar to the ones showed for c_{500} , for example increasing the correlation when only U and P clusters are considered.

It is remarkable that the only parameter that correlates very well with H_Z is r'_c (with a Pearson coefficient of 0.972). The theory states that the natural tendency of a gravitational system towards its evolution is establishing a structure core-halo. This is exactly what the correlation of H_Z and r'_c may be

suggesting: the core radius grows with the entropy of the cluster.

We consider that H_Z is an efficient parameter for estimating the relaxation/dynamical state of galaxy clusters, maybe better than the the others we have compared in this not complete exercise, because it can capture more important aspects of such evolutionary snapshot. However, it is important to note that no parameter can, alone, account for all the evolutionary aspects such as interaction with the cosmological environment, collapse and mass growth, galaxy formation, AGN activity, feedback processes, among others, making paramount to consider different observations and analyses for constructing the most complete picture as possible.

7. DISCUSSION AND CONCLUSIONS

In this work we have proposed an entropy estimator, H_Z , which can be calculated from global dynamical parameters (virial mass, projected virial radius and velocity dispersion), to characterize the dynamical state of galaxy systems. Initially, a slight modification of the standard $T ds$ Gibbs relation was carried out to include the peculiar behavior of self-gravitating systems and, as a result, an expression was obtained for the entropy component s related only to the galaxy ensemble, which is a function of the internal kinetic energy and the volume of the systems.

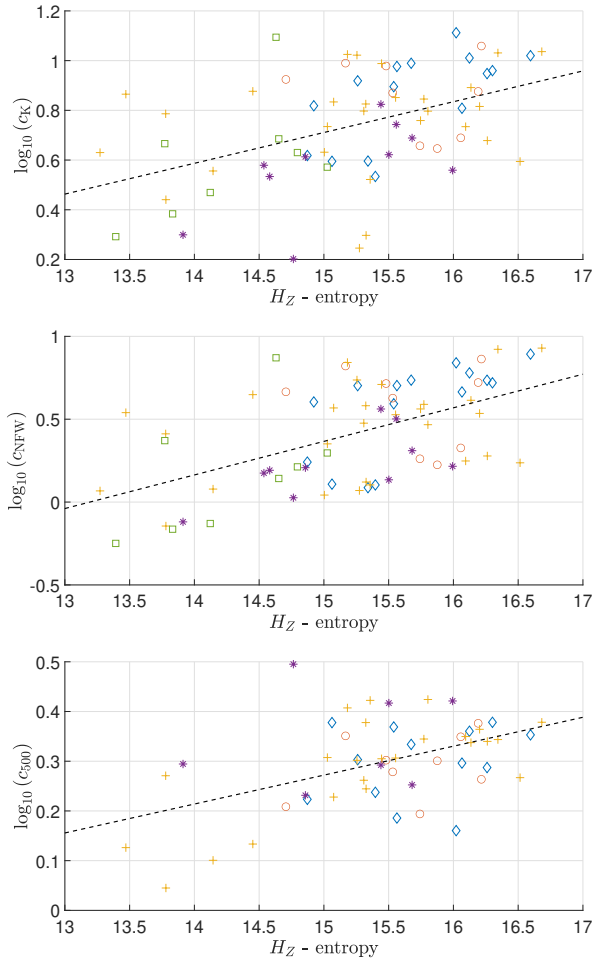


Fig. 8. Scatterplots of H_Z -entropy *vs.* concentration indices (c_K , c_{NFW} , and c_{500}) for the *Top70* cluster sample. The symbols used for the markers have the same meaning as in Fig. 5. The dashed line represents the best linear fit to the data, with \mathcal{R}^2 of 0.203, 0.264 and 0.215, respectively from top to bottom.

The direct association of the H_Z -entropy estimator to the dynamical state of the galaxy systems comes from the second law of thermodynamics, according to which entropy increases as the systems advance towards more stable states, reaching a local maximum in virial equilibrium. This does not assert that the galaxy system reaches a stable state of equilibrium, which would be determined by a global maximum of entropy, but rather a state of greater stability than its previous evolutionary configurations, the so-called dynamical relaxation. Thus, although the virial theorem is fulfilled in relaxed states with local entropy maximum, these are *metastable equilibria* that can be broken if the galaxy system significantly interacts with its environment, such as through ac-

cretions and mergers with other systems. However, if the system is isolated (or its interaction with the environment is negligible), its entropy value remains in the vicinity of the maximum and its behavior in such state will be indistinguishable from dynamical relaxation.

In order to evaluate the power of this entropy to represent the evolutionary state of a galaxy system, we correlated it to four independent estimators: two observational and two statistical. The two observational come from analyses of the internal structure of real clusters, particularly the discrete gravitational assembly state (obtained from optical data) and three continuous concentration indices (both from optical and X-ray data), applied to a sample of 70 well spectroscopically-sampled nearby galaxy clusters. The statistical estimators comprehend the Shannon (information) entropy and the relaxation probability, calculated for the same sample of observed clusters and for a sample of 248 halos (simulated clusters) from IllustrisTNG.

The first striking result of our analysis is that the H_Z -entropy correlates very well with the gravitational assembly state of the clusters obtained from observational optical data. The H_Z -entropy increases with the decrease in the level of substructuring, which is interpreted as the less relaxed a cluster is, more information is lost when treating it as a virialized system. Specifically, both U and P clusters show the highest entropies, while L present the lowest values for this property. Since P clusters are massive, while possessing only low significance substructures (low mass accretions), they resemble the unimodal U clusters. On their turn, L clusters are, as pointed by Caretta et al. (2023), the ‘less evolved’, in the sense that they are the poorest, less massive and have not suffered significant merging processes yet. S and M clusters present a large range in entropies. This happens because both less or more massive clusters (and both less and more evolved ones) can suffer new mergings or accretion at any time.

The H_Z -entropy estimator was derived based on specific variables (*e.g.*, per mass unit), which allows comparisons between galaxy systems of different masses (\mathcal{M}_{vir}) and sizes (R_{vir}). Moreover, equation (12) shows a clear functional dependence of the entropy on the galaxy velocity dispersion (*i.e.*, on the specific internal kinetic energy $\kappa = (\alpha/2)\sigma_{\text{LOS}}^2$ of the galaxy ensemble). This implies that although groups and poor clusters can reach virial equilibrium like rich clusters, the relaxation state of the latter will be characterized by higher entropy values given their higher velocity dispersions. It is possible to ver-

ify that, by calculating H_Z without taking into account the term that depends on σ_{LOS} in (12), then the entropy values of all sampled clusters are very closely distributed around a central value $\langle H_Z \rangle$ that depends on the units chosen for \mathcal{M}_{vir} and R_{vir} .

A possible evolutionary line between systems at different assembly levels has been schematized in Figure 9. Multimodal (M) systems could be formed by the merger of two or more low-mass unimodal (L) systems. These mergers increase the entropy level of the systems due to the increase in mass and number of particles (*i.e.*, galaxies). As gravity further assembles the fused parts, a main structure is formed in the clusters, and, when still dynamically significant substructures remain, we have substructured systems (S). In this process, the entropy increases because the main structure, which is larger than the rest of the substructures, begins a virialization process and dominates the dynamics of the cluster. The substructures are special configurations in the distribution of galaxies, macroscopic movements that can slightly affect the dynamics of the system. However, these are little by little accreted and dissolved by the main structure, until they become less significant and the clusters evolve marginally towards the more assembled states primaries (P) and unimodals (U), where the entropy is greater given the large homogeneity in the distribution of galaxies, large velocity dispersion and the proximity to virialization.

It is important to highlight that, despite the notable tendency of H_Z -entropy to increase with the $L \rightarrow M \rightarrow S \rightarrow P/U$ sequence of assembly states, an individual cluster could not be assigned to a specific \mathcal{A} class only knowing its H_Z -entropy value, since this classification requires the knowledge of more observational (optical and X-ray) features of the cluster. However, the H_Z -entropy values allow us to know statistically which clusters are likely to be more relaxed—and probably with a higher assembly level—than others when working with a large sample of clusters, *e.g.*, as in the case of the *Top70* or *TNG300* sample. In addition, if by qualitative methods two clusters appear similar, their H_Z values can help to discriminate if they are at the same evolutionary state or if one of them is more advanced (or delayed) than the other, like is the case of L and U clusters.

Resuming the question about unimodal clusters, we have also verified that L clusters lack the core-halo spatial configuration, unlike U clusters that exhibit a clear central concentration of galaxies. In fact, as can be seen from the galaxy concentration indices, U clusters generally achieve the highest concentration indices while L clusters have the lowest.

Thus, the Hellinger distance between the respective *observed* and *relaxed PDFs* of a cluster become larger when the latter lack a central concentration.

Concerning the statistical estimators we used to test H_Z -entropy, we found that the Shannon—or information—entropy H_S presents a remarkable (almost linear) correlation with it.

Information entropy does not necessarily have a simple correspondence with physical entropy, but we can provide a possible explanation for the correlation between the H_Z and H_S entropies as follows. Given that the cylinder of x -points of observational data constitutes a projected phase-space (*e.g.*, it contains 2D-position and 1D-velocity coordinates of particles in a system that evolves with time) for each cluster, $\bar{f}_{r\theta z}$ is like a ‘coarse-grained distribution function’ obtained for a fixed time—the observing time—in this phase-space. Thus, the Shannon entropy $H_S(\bar{f}_{r\theta z})$ meets in this context the criteria to be a H-function (see, Tremaine, Hénon & Lynden-Bell 1986, do not confuse with the Hellinger distance in (22)) and, therefore, it always increases with the evolution of the galaxy ensemble.

On the other hand, the argument $\kappa^{\alpha/2}v^{-1}$ in (11) is equivalent, by analogy with statistical mechanics concepts, to the \mathcal{Z} partition function of the galaxy ensemble. Every \mathcal{Z} function is defined in the phase-space of a system (*e.g.*, Hill 1956; Landau & Lifshitz 1980), taking higher values in states of—or close to—equilibrium, where dynamical relaxation increases the randomness in the particle distribution and offers a greater number of ways in which energy can be distributed inside the system, *i.e.*, in states of higher entropy since $s \propto \mathcal{Z}$. The $\bar{f}_{r\theta z}$ distributions and \mathcal{Z} functions are intrinsically related in the thermodynamic limit of a system (*e.g.*, Jaynes 1957), even in self-gravitating ones (*e.g.*, Chavanis 2003, 2006), reason why both H_Z and H_S are related between them and to the dynamical state of the galaxy ensemble, and allow us to measure how close it is to virial equilibrium.

This interpretation is reinforced by the relaxation probability \mathcal{P}_{relax} which shows that the closer the galaxy cluster is to the virialization, smaller is the distance between its observed distribution of galaxies and the expected theoretical equilibrium one.

The entropy estimations presented here are very promising because, once one has a representative sample of galaxy members for the cluster, the calculation of the input parameters is straight forward. This low-cost analysis is much easier than the broader one presented in Caretta et al. (2023), and can also be used as a complementary analysis in the

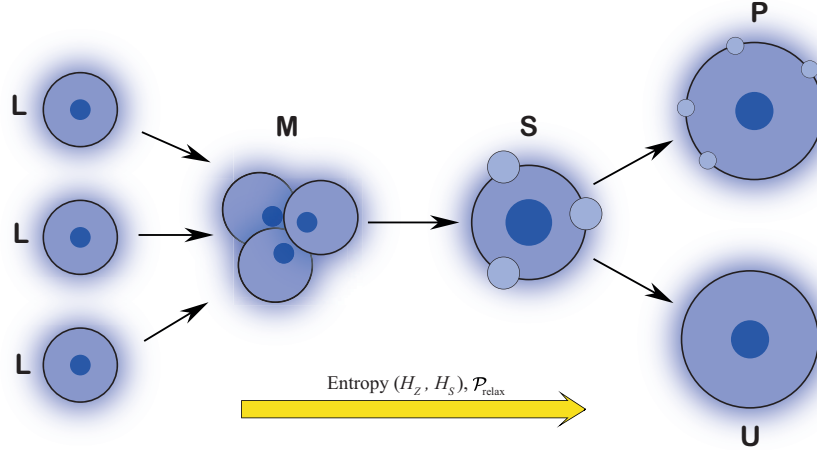


Fig. 9. Diagram of a possible evolutionary line between systems in the different assembly levels (U-P-S-M-L). The entropy levels of the galaxy systems, obtained using the H_Z and H_S estimators, increase as they progress towards more dynamically relaxed states (with a higher probability of relaxation, $\mathcal{P}_{\text{relax}}$), *i.e.*, states with more homogeneous and less substructured galaxy distributions (or where the substructures are insignificant for the dynamics of the systems).

study of the assembly state of the galaxy systems. It is still lacking a deeper analysis of the implications of the results presented here, what we plan to do in a future work. We also intend to extend this analysis to other scales of galaxy clustering, especially in the direction of the evolution of the large scale structures like the superclusters of galaxies.

Our main conclusions are the following:

- The H_Z -entropy estimator, which depends solely on observational (optical) parameters, adequately captures the entropy of clusters manifested in the (spatial and velocity) distribution of their member galaxies.
- The H_Z -entropy is related, through the second law of thermodynamics, with the evolutionary state of galaxy systems. Entropy increases as systems evolve towards more stable states, reaching a local (non-unique) maximum at virial equilibrium.
- There is a significant correlation between the H_Z -entropy of galaxy systems and their gravitational assembly states (\mathcal{A} , Caretta et al. 2023), presenting an entropy growth in the $L \rightarrow M \rightarrow S \rightarrow P/U$ sequence, direction in which the relaxation probability $\mathcal{P}_{\text{relax}}$ of the clusters also increases.
- There is a remarkable (almost linear) correlation between H_Z -entropy and the Shannon (information) entropy, H_S , reinforcing that the dynamical

cal entropy we propose can capture the increase in disorder and loss of information in the process of virialization.

- Clusters with higher velocity dispersions of member galaxies tend to have higher H_Z and H_S entropy values, indicating more random galaxy distributions.
- The H_Z -entropy estimator shows a great capacity to capture the state of relaxation and evolution of the galaxy systems, maybe larger than the one presented by other conventional continuous parameters used for this purpose.
- The H_Z -entropy estimator provides valuable information on the dynamical state and assembly levels of galaxy clusters, which may have significant applications in studying the evolution of galaxy systems and understanding their dynamics.

Acknowledgments

The authors JMZ, CAC and EGM thank financial support from *Universidad de Guanajuato* (DAIP), *Convocatoria Institucional de Investigación Científica*, projects 096/2021 and 162/2022. JMZ acknowledges funding from CONACyT PhD grant and appreciates the manuscript revision by Manuela Paz. APG acknowledges support from *Departamento de Matemáticas, Universidad del Cauca*. The authors are grateful to Dr. Roger Coziol and Dr. Francisco

Escamilla for the discussions that helped to improve the manuscript.

REFERENCES

- Abell, G. 1958, *ApJS*, 3, 211
- Abell, G., Corwin, H. G. Jr., & Olowin, R. P. 1989, *ApJS*, 70, 1
- Adami, C., Mazure, A., Katgert, P., & Biviano, A. 1998, *A&A*, 336, 63
- Andrade-Santos, F., Lima-Neto, G. B., Laganá, T. F. 2012, *ApJ*, 746, 139
- Andrade-Santos, F., Jones, C., Forman, W. R., et al. 2017, *ApJ*, 843, 76
- Antonov, V. A. 1962, *Vest. Leningrad Univ.* 7, 135 (Translated, 1985, in Goodman J., Hut P., eds, *Proc. IAU Symp. 113, Dynamics of star clusters*. Reidel, Dordrecht, p. 525)
- Araya-Melo, P., Reisenegger, A., Meza, A., van de Weygaert, R., Dünner, R., & Quintana, H. 2009, *MNRAS*, 399, 97
- Bahcall, N. A. 1996, preprint (arXiv:astro-ph/9611148v1)
- Balberg, S., Shapiro, S. L., & Inagaki, S. 2002, *ApJ*, 568, 475
- Bautz, L. P., & Morgan, W. W. 1970, *ApJ*, 162, L149
- Beers, T. C., Flynn, K., & Gebhardt, K. 1990, *AJ*, 100, 32
- Binney J., & Tremaine, S. 2008, *Galactic Dynamics* (2nd ed.; Princeton, NJ: Princeton University Press)
- Biviano, A., Murante, G., Borgani, S., Diaferio, A., Dolag, K., & Girardi, M. 2006, *A&A*, 456, 23
- Böhringer, H., & Werner, N. 2010, *A&A Rev.*, 18, 127
- Böhringer, H., & Chon, G. 2021, *A&A*, 656, A144
- Bravo-Alfaro, H., Caretta, C. A., Lobo, C., Durret, F., & Scott, T. 2009, *A&A*, 495, 379
- Bryan, G. L., & Norman, M. L. 1998, *ApJ*, 495, 80
- Buote, D. A., & Tsai, J. C. 1995, *AJ*, 452, 522
- Caretta, C. A., Andernach, H., Chow-Martínez, M., Coziol, R., et al. 2023, *RMxAA*, 59, 345
- Carlberg, R. G., et al. 1996, *ApJ*, 462, 32
- Carlberg, R. G., et al. 1997a, *ApJ*, 476, L7
- Carlberg, R. G., et al. 1997b, *ApJ*, 485, L13
- Cavagnolo, K. W., Donahue M., Voit G. M., Sun M. 2009, *ApJS*, 182, 12
- Cautun, M., van de Weygaert, R., Jones, B. J. T., Frenk, C. S. 2014, *MNRAS*, 441, 2923
- Chavanis, P. H., Rosier, C., & Sire, C. 2002, *Phys. Rev. E*, 66, 036105
- Chavanis, P. H. 2003, *A&A*, 401, 15
- Chavanis, P. H. 2006, *International Journal of Modern Physics B*, Vol. 20, 22, 3113
- Cohn, H. 1980, *ApJ*, 242, 765
- Cover, T. M., & Thomas, J. A. 2006, *Elements of Information Theory* (2nd ed.; Hoboken, NJ: Wiley-Interscience)
- Davis, M., Efstathiou, F., Frenk, C. S., & White, S. D. M., 1985, *ApJ*, 292, 371
- Dehnen, W. 1993, *MNRAS*, 265, 250
- Dehnen, W. 2005, *MNRAS*, 360, 892
- Diemer, B. 2023, *MNRAS*, 519, 3292
- Dressler, A., & Shectman, S. A., 1988, *AJ*, 95, 985
- Einasto, J. 1965, *Kinematics and dynamics of stellar systems*, *Trudy Inst. Astrofiz. Alma-Ata*, 5, 87
- Einasto, J., Klypin, A., Saar, E., & Shandarin, S., 1984, *MNRAS*, 206, 529
- Einasto, J. 2010, *AIP Conference Proceedings*, 1205, 72
- Felder, C. E., Mao, Y.-Y., Zentner, A. R., Newman, J. A., Wu, H.-Y., Wechsler, R. H. 2020, *MNRAS* 499, 2426
- García-Manzanárez, E. 2022, MSc. Thesis, Universidad de Guanajuato, Mexico
- Geller, M. J., & Beers, T. C., 1982, *PASP*, 94, 421
- Geller, M. J., & Huchra, J. P., 1989, *Science*, 246, 897
- Gibbons, J. D., & Chakraborti, S. 2003, *Nonparametric Statistical Inference* (4th ed.; New York: Marcel Dekker)
- Girardi, M., & Mezzetti, M. 2001, *ApJ*, 548, 79
- Gunn, J. E., & Gott III, J. R. 1972, *ApJ*, 176, 1
- Hellinger, E. 1909, *Journal für die reine und angewandte Mathematik*, 136, 210
- Hernquist, L. 1990, *AJ*, 356, 359
- Heuman, C., & Shalabh, M. S. 2016, *Introduction to Statistics and Data Analysis* (Springer)
- Hill, T. L. 1956, *Statistical Mechanics* (New York: McGraw-Hill)
- Imre, A. R. 2007, How to generate and measure negative pressure in liquids? in *NATO Science Series II: Mathematics, Physics and Chemistry*. Vol 242, *Soft Matter under Exogenic Impacts*, eds. S. J. Rzoska & V. A. Mazur (Dordrecht: Springer), 379
- Iqbal, N., Ahmad, F., & Khan, M. S. 2006, *J. Astrophys. Astron.*, 27, 373
- Iqbal, N., Khan, M. S., & Masood, T. 2011, *Natural Science*, 3, 1
- Jaynes, E. T. 1957, *Physical Review*, 106, 4
- Jones, C., & Forman, W. 1984, *ApJ*, 276, 38
- Kashibadze, O. G., Karachentsev, I. D., & Karachentseva, V. E. 2020, *A&A*, 635, A135
- King, I. R. 1962, *AJ*, 67, 471
- Laganá, T. F., Durret, F., & Lopes, P. A. A. 2019, *MNRAS*, 484, 2807
- Landau, L. D., & Lifshitz, E. M. 1980, *Statistical Physics, Course of Theoretical Physics*. Vol. 5 (3rd ed.; Butterworth-Heinemann)
- Libeskind, N. I., et al. 2018, *MNRAS*, 473, 1195
- Lifshitz, E. M., & Pitaevskii, L. P. 1981, *Physical Kinetics* (Oxford: Pergamon)
- Lima-Neto, G. B. 2005, *Brazilian Journal of Physics*, 35, 4B
- Limber, D. N., & Mathews, W. G. 1960, *ApJ*, 132, 286
- Lokas, E. L., & Mamon, G. A. 2003, *MNRAS*, 343, 401
- Lovisari, L., Forman, W., Jones, C., et al. 2017, *ApJ*, 846, 51
- Lynden-Bell, D. 1967, *MNRAS*, 136, 101
- Lynden-Bell, D., & Wood, R. 1968, *MNRAS*, 138, 495
- Lynden-Bell, D., & Lynden-Bell, R. 1977, *MNRAS*, 181,

405

- Navarro, J. F., Frenk, C. S., & White, S. D. M. 1996, *ApJ*, 462, 563
- Nelson, D., et al. 2019, *Computational Astrophysics and Cosmology*, 6, 2
- Oort, J. H. 1983, *ARA&A*, 21, 373
- Padmanabhan, T. 1989, *ApJS*, 71, 651
- Padmanabhan, T. 1990, *Phys. Rep.*, 188, 5
- Padmanabhan, T. 1993, *Structure formation in the Universe* (Cambridge: Cambridge University Press)
- Padmanabhan, T. 2000, *Theoretical Astrophysics. Vol. I, Astrophysical Processes* (Cambridge: Cambridge University Press)
- Parekh, V., van der Heyden, K., Ferrari, C., et al. 2015, *A&A*, 575, A127
- Peebles, P. J. E. 1980, *The Large-Scale Structure of the Universe*. (Princeton, NJ: Princeton University Press)
- Pontzen, A., & Governato, F. 2013, *MNRAS*, 430, 121
- Planck Collaboration: Ade, P. A. R., et al. 2016, *A&A*, 594, A27
- Rood, H. J., Page, T. L., Kintner, E. C., & King, I. R. 1972, *ApJ*, 175, 627
- Sampaio, F. S., & Ribeiro, A. L. B. 2014, *New Astronomy*, 27, 41
- Santiago-Bautista, I., Caretta, C. A., Bravo-Alfaro, H., Pointecouteau, E., & Andernach, H. 2020, *A&A*, 637, A31
- Sarazin, C. L. 1988, *X-ray Emission from Clusters of Galaxies* (Cambridge University Press)
- Saslaw, W., 1980, *ApJ*, 235, 299
- Saslaw, W., & Hamilton, A. 1984, *ApJ*, 276, 13
- Schneider, P. 2015, *Extragalactic Astronomy and Cosmology: An Introduction* (2nd ed.; Springer)
- Shannon, C. E. 1948, *Bell Syst. Tech. J.* 27, 379
- Springel, V., et al. 2005, *Nature*, 435, 629
- Springel, V., et al. 2018, *MNRAS*, 475, 676
- Tozzi P., Norman C. 2001, *ApJ*, 546, 63
- Tremaine, S., Hénon, M., & Lynden-Bell, D., 1986, *MNRAS*, 219, 285
- Tully, R. B. 2015, *AJ*, 149, 54
- Voit, G. M. 2005, *Reviews of Modern Physics*, 77, 207
- White, S. D. M. 1992, in *Clusters and Superclusters of Galaxies*, ed. A. C. Fabian (Dordrecht: Kluwer), 17
- White, S. D. M. 1996, preprint (arXiv:astro-ph/9602021v1)
- Zakhochay, V. A. 2018, *Odessa Astronomical Publications*, 30, 56
- Zhang, Y.-Y., Andernach, H., Caretta, C. A., et al. 2011, *A&A*, 526, A105
- Zhang, Y.-Y., Reiprich, T. H., Schneider, P., et al. 2017, *A&A*, 599, A138

Johan M. Zúñiga: Departamento de Astronomía, Universidad de Guanajuato, Apartado Postal 36000, Guanajuato, Gto., México (jm.zuniga@ugto.mx).